

1 **Hf-Zr anomalies in clinopyroxene from mantle xenoliths from**
2 **France and Poland: implications for Lu-Hf dating of spinel**
3 **peridotite lithospheric mantle**

4 Hilary Downes¹, Caja de Vries¹ and Nadine Wittig²

5 1. Department of Earth and Planetary Sciences, Birkbeck University of London, Malet
6 Street London WC1E 7HX UK.

7 2. Department of Earth Sciences, Carleton University, Ottawa, Ontario, K1S 5B6
8 Canada

9

10

11 **ABSTRACT**

12 Clinopyroxenes in some fresh anhydrous spinel peridotite mantle xenoliths from the
13 northern Massif Central (France) and Lower Silesia (Poland), analysed for a range of
14 incompatible trace elements by Laser Ablation-Inductively Coupled Plasma Mass
15 Spectrometry, show unusually strong negative anomalies in Hf and Zr relative to
16 adjacent elements Sm and Nd, on primitive-mantle-normalised diagrams. Similar Zr-Hf
17 anomalies have only rarely been reported from clinopyroxene in spinel peridotite
18 mantle xenoliths worldwide, and most are not as strong as the examples reported here.
19 Low Hf contents give rise to a wide range of Lu/Hf ratios, which over geological time
20 would result in highly radiogenic ϵ_{Hf} values, decoupling them from ϵ_{Nd} ratios. The
21 high $^{176}\text{Lu}/^{177}\text{Hf}$ could in theory produce an isochronous relationship with $^{176}\text{Hf}/^{177}\text{Hf}$
22 over time; **an errorchron** is shown **by clinopyroxene from mantle** xenoliths from the
23 northern Massif Central. However, in a review of the literature, we show that most
24 mantle spinel peridotites do not show such high Lu/Hf ratios in their constituent
25 clinopyroxenes, because they lack the distinctive Zr-Hf anomaly, and this limits the
26 usefulness of the application of the Lu-Hf system of dating to garnet-free mantle rocks.
27 **Nevertheless, some mantle xenoliths from Poland or the Czech Republic** may be
28 amenable to Hf-isotope **dating in the future.**

29

30 **Keywords:** mantle, spinel peridotite, clinopyroxene, France, Poland, Lu-Hf
31 geochronology

32

33 **1. DATING EVENTS WITHIN THE UPPER MANTLE**

34 Methods have long been sought that can date events which have occurred within the
35 shallow (spinel peridotite) subcontinental lithospheric mantle. Success has been
36 achieved in those rare mantle rocks that contain zircon (e.g. Sanchez-Rodriguez and
37 Gebauer 2000; Femenias et al., 2003; Zheng et al., 2006), probably related to
38 enrichment in the lithosphere by silicate melts. Osmium isotope methods based on
39 model ages or Re-depletion ages can provide a guide to the age of mantle events (e.g.
40 Pearson et al., 2002; Schmidt and Snow, 2002; Handler et al., 2003; Widom et al.,
41 2003; Xu et al., 2008; Rudnick and Walker, 2009; Janney et al., 2010; Wittig et al.,
42 2010a; Wittig et al., 2010b) but are best applied to regions of ancient lithospheric
43 mantle. The Sm-Nd isotope system can be used to determine model ages, but this
44 system is strongly affected by mantle metasomatism, leading to mixed ages that are
45 probably meaningless (Zangana, 1995). Notable exceptions are the “approximate
46 isochron” shown by clinopyroxenes from mantle xenoliths from Inner Mongolia (Deng
47 and Macdougall, 1992) and errorchrons shown by minerals from mantle spinel
48 peridotite xenoliths from Jordan (Nasir and Rollinson, 2009).

49 In contrast, the Lu-Hf system may provide a more robust method of dating mantle
50 lithologies, particularly of garnet peridotites, garnet pyroxenites and eclogites (e.g.,
51 Schmidberger et al., 2002, 2007; Ionov 2004; Lazarov et al., 2009; Gonzaga et al.,
52 2010; Shu et al., 2013). Its decay scheme (^{176}Lu decays to ^{176}Hf with decay constant of
53 $1.865 \times 10^{-11} \text{ yr}^{-1}$ (Scherer et al., 2001; Söderlund et al., 2004)) is suitable for dating
54 ancient mantle events, and it is less prone to respond to metasomatism, because many
55 potential metasomatic agents have low Lu and Hf contents. Since Lu is a heavy rare
56 earth element, it shows greater compatibility with the mantle compared to Hf, which
57 has a compatibility similar to that of Sm and Nd during mantle melting. The question

58 then arises as to whether Lu-Hf isotopic system could be appropriately applied to
59 garnet-free mantle peridotite samples.

60 Clinopyroxene is the main host of most incompatible lithophile trace elements in the
61 garnet-free anhydrous lithospheric mantle. Dobosi et al (2010) has shown in a study of
62 Pannonian Basin mantle peridotite xenoliths that the abundances of incompatible trace
63 elements in mantle clinopyroxenes are usually much greater (by an order of magnitude
64 or more) than those in coexisting orthopyroxenes, and that the abundances of Lu, Hf,
65 Zr, Sm and Nd in clinopyroxene always exceed those in orthopyroxene. Hence for
66 technical reasons, it is not possible to use the other minerals in a mantle xenolith to
67 derive an internal mineral isochron.

68 Figure 1 shows a compilation of Lu/Hf and Sm/Nd ratios from clinopyroxenes in
69 mantle spinel peridotites worldwide. It demonstrates that the range of Lu/Hf ratios
70 reported for mantle clinopyroxenes is much greater than the range in Sm/Nd. There is a
71 “common mantle clinopyroxene” field with Sm/Nd ratios of 0.2-0.4 and Lu/Hf ratios of
72 0.1-0.3. This field is centered on the value for Lu/Hf and Sm/Nd in primitive mantle
73 (Sun and McDonough 1989). However, in other mantle samples, Sm/Nd ratios in
74 clinopyroxene rarely exceed 0.7 whereas Lu/Hf ratios greater than 1 are not unknown.
75 Thus Hf model ages and Lu-Hf isochrons might theoretically be derived from these
76 garnet-free samples that have experienced depletion events and were not overwritten by
77 metasomatic addition of Lu or Hf to the lithospheric mantle. In this study, we report the
78 trace element compositions of clinopyroxenes in a variety of four-phase anhydrous
79 mantle spinel peridotite xenoliths from France and SW Poland that show a wide range
80 of Lu/Hf ratios, resulting from variable depletion in Hf. We compare them to
81 clinopyroxenes from mantle spinel peridotites worldwide and show that only a very
82 small proportion of clinopyroxenes in garnet-free mantle rocks have experienced
83 sufficient fractionation of Hf from Lu to be amenable to dating by this method.

84

85 2. METHODOLOGY AND SAMPLES ANALYSED

86 Forty-three spinel peridotite mantle xenoliths from Neogene alkali basalts of the French
87 Massif Central were analysed. Petrological details, **sample localities** and major element
88 compositions have been discussed extensively elsewhere (Downes and Dupuy 1987;
89 Zangana et al., 1998; Downes et al., 2003). **They are all Cr-diopside and** contain no
90 hydrous minerals. **Clinopyroxene from xenoliths from the northern domain have lower**
91 **TiO₂ and Na₂O contents (<0.5 wt% and <1.2 wt%, respectively) than those from the**
92 **southern domain (Downes et al., 2003), suggesting more extensive depletion in the**
93 **northern domain mantle.** Trace element abundances in clinopyroxenes from some of
94 these samples had been analysed previously by different methods and in different
95 laboratories (Downes and Dupuy 1987; Vannucci et al., 1994; Zangana et al., 1998;
96 Mason et al., 1999; Downes et al., 2003). Clinopyroxene grains were hand-picked from
97 these samples, usually from the medium grain size fraction (850-425 µm). In addition,
98 separated clinopyroxene from sixteen spinel peridotite mantle xenoliths from the
99 Neogene alkali basalts in the Polish Sudetes (Lower **Silesia – localities Ladek, Lutynia**
100 **and Wilcza Gora**) were provided by Dr J Blusztajn and correspond to the samples
101 previously described by Blusztajn and Shimizu (1994). **These clinopyroxene are also**
102 **Cr-diopsides and have low TiO₂ and Na₂O contents similar to those of the Northern**
103 **Massif Central domain.** Similar material has been studied more recently by Matusiak-
104 Malek et al (2010) and Puziewicz et al. (2011). Up to eight grains per sample were
105 analysed, with a minimum of 3 points per grain; the results were averaged for each
106 sample. **No differences between cores and rims were detected.**

107 Trace element compositions were determined by in situ laser ablation inductively
108 coupled plasma mass spectrometry (LA-ICPMS) at Birkbeck/UCL. The analytical
109 instrumentation consists of a New Wave Research YP213 laser aperture imaged
110 frequency quintupled Nd:YAG solid state laser source, operating at a wavelength of
111 213 nm, coupled to an Agilent 7500a quadrupole ICP-MS. A 50 micron laser spot size
112 was used. Time-resolved analysis was employed during data acquisition. The samples
113 were ablated with pulses of 80mJ at a pulse repetition rate of 5Hz, over an ablation time
114 of 20 s. The synthetic glass reference material NIST 612 was used as a calibration
115 standard with the average composition of Pearce et al. (1997). Ca contents of
116 clinopyroxenes analysed by electron microprobe were used for internal calibration to

117 correct for differences in ablation characteristics between samples and standards. The
118 GEMOC Glitter reduction software was used to process the raw data. This program
119 provides minimum detection limits for all elements in each individual analysis, and the
120 data reported were all above the relevant detection limit. Any results that were below
121 detection limit (a common case with Rb and Ba concentrations in mantle
122 clinopyroxenes) are shown in the Tables as a blank.

123 An in-house standard RP91-17, a clinopyroxene from a mantle xenolith from the
124 southern French Massif Central (Zangana et al., 1998), was used to ensure
125 comparability with previously determined values by LA-ICPMS (Mason et al., 1999)
126 who also used the NIST 612 international standard. Trace element compositions of
127 clinopyroxenes from the Massif Central are given in Table 1, together with data for the
128 in-house standard; those for clinopyroxene from mantle xenoliths from Poland are
129 given in Table 2. In general the comparability between our results for RP 91-17 and
130 those of Mason et al (1999) are very good, i.e. within 1-2%, but there is a significant
131 discrepancy for Pb concentrations (our value = 0.38 ppm; that of Mason et al (1999) is
132 1.5 ppm). We consider that this may be due to a memory effect in the earlier analysis,
133 as the same standard clinopyroxene analysed using the LA-ICPMS facility at Kingston
134 University yielded a value of 0.17 ppm Pb. Comparisons of our LA-ICPMS Lu and Hf
135 analyses with concentrations given by Wittig et al (2006) on bulk clinopyroxenes by
136 isotope dilution (ID) are generally good despite ID being inherently a more precise
137 method (e.g. for sample Mb50, Lu = 0.1277 ppm by ID and 0.12 ppm by LA-ICPMS;
138 Hf = 0.032 ppm by ID and 0.02 ppm by LA-ICPMS). Discrepancies may also be due to
139 the different volumes of material that are analysed by the two different methods, with
140 ID analysing much larger volume of clinopyroxene.

141

142 **3. TRACE ELEMENT VARIATIONS IN CLINOPYROXENES FROM SPINEL** 143 **PERIDOTITES**

144 It has been recognized that the sub-continental mantle lithosphere beneath the French
145 Massif Central is separated into a northern and southern domain characterized by
146 contrasting bulk rock compositions of mantle xenoliths (Lenoir et al., 2000),

147 clinopyroxene compositions (Downes et al., 2003) and geophysical signatures (Babuska
148 et al., 2002). The mantle xenoliths from the Massif Central have therefore been divided
149 into those two geographic groups, which also correspond to differences in their trace
150 element patterns. Clinopyroxenes in xenoliths from the southern region (samples prefixed
151 by RP, Bo, Ta, Gr, Ce, Vp, Pey, BR, Ms, AL and Z in Table 1), tend to show flat trace
152 element patterns (Fig. 2), when normalised to primitive mantle (Sun and McDonough
153 1989). Their Zr/Hf ratios are mostly in the range 23 to 44, i.e. approximately chondritic
154 (36), although a very small number of analyses have strongly sub-chondritic values (3-
155 13). In contrast, clinopyroxenes from northern localities (Mb, PH, FR, Bt, St and CH in
156 Table 1) tend to show highly spiked patterns, with several samples showing particularly
157 strong negative anomalies in Zr and Hf (Fig. 2). These samples also show positive
158 anomalies in Sr, Pb, La and U compared to adjacent elements, and strong enrichment in
159 LREE over MREE. The Zr/Hf ratios of these unusual clinopyroxenes vary from strongly
160 subchondritic to suprachondritic (0.5 to 82). Some of the variation may be a result of
161 analytical problems, given that the Hf content of these minerals is conspicuously low
162 (less than 0.05 ppm).

163 Clinopyroxenes from mantle xenoliths from SW Poland (Fig. 3) also show a variety of
164 trace element patterns, although there is no clear correlation with location. Our trace
165 element results are similar to those of Matusiak-Malek et al (2010) for different samples
166 from similar localities. In general they are more enriched in the LREE than the Massif
167 Central samples, and show conspicuous troughs at Ta and Pb. However, some also show
168 conspicuous negative anomalies in Zr and Hf, although these are not as strong as those
169 seen in mantle clinopyroxenes from the northern Massif Central. Their Zr/Hf ratios are in
170 the range 3-151. The Polish samples appear to show significant decoupling of Ta
171 relative to Nb. Similar low Ta values are also shown in clinopyroxenes from Polish
172 mantle xenoliths analysed by Matusiak-Malek et al. (2010), but unfortunately Nb
173 was not analysed in that study. Although this is beyond the scope of this paper, the
174 superchondritic Nb/Ta values in the Polish mantle clinopyroxenes are worthy of
175 further investigation.

176 Further examples of Zr-Hf-depleted clinopyroxenes have been found in spinel peridotite
177 xenolith suites from elsewhere in Europe (Fig. 4), namely Monte Vulture in southern Italy
178 (Downes et al., 2002), the Hyblean Plateau in Sicily (Perinelli et al., 2008) and the
179 Bohemian massif **within the Czech Republic** (Ackerman et al., **in press**). Such strong
180 Zr-Hf anomalies are uncommon in clinopyroxene from mantle peridotites worldwide,
181 although other examples (Fig. 4) have been reported from peridotite xenoliths from the
182 Bearpaw Mountains, Montana (Downes et al., 2004) and Tok, Siberia (Ionov et al.,
183 2006). **Clinopyroxene from a mantle xenolith from the Avacha volcano in Kamchatka**
184 **situated above an active subduction zone** (Halama et al., 2009), **shows similarly low Hf**
185 **abundances but does not show the same extent of Lu/Hf fractionation.**

186

187 **4. Hf ISOTOPE COMPOSITIONS OF CLINOPYROXENES IN SPINEL** 188 **PERIDOTITES**

189 Mantle peridotite clinopyroxenes analysed in this study display a range of Lu contents
190 from 0.05 to 0.45 ppm, whereas their Hf contents range from 0.01 to 2.5 ppm. Worldwide
191 mantle peridotite clinopyroxenes show similar ranges in Lu and Hf (although samples
192 from Tok in Siberia (Ionov et al., 2006a) show even higher Hf contents, up to 5.65 ppm,
193 that are not accompanied by high Lu contents). There is a broad but very poor positive
194 correlation between Lu and Hf contents in mantle clinopyroxenes (not shown). Figure 5
195 shows the Lu/Hf ratios of our samples plotted as a function of Hf content, compared with
196 a worldwide data set of mantle peridotite clinopyroxene compositions. **We have included**
197 **clinopyroxene from a mantle xenolith from Avacha volcano (Halama et al., 2009),**
198 **situated above an active subduction zone, for comparison.** Only clinopyroxenes that
199 contain less than 0.1 ppm Hf show high Lu/Hf ratios, ranging from 1 to 100. A wide
200 range of Lu/Hf ratios would be a prerequisite for dating mantle events using the Lu-Hf
201 method. Only a suite of mantle peridotite samples that includes clinopyroxenes with
202 high Lu/Hf ratios, such as those from the northern Massif Central, would be
203 amenable to Lu-Hf isotopic age dating, and then only if neither Lu nor Hf had been
204 added to the sample by later events such as metasomatism.

205 Methodology and results for Hf isotope compositions in clinopyroxenes from a subset
206 of Massif Central spinel peridotite xenoliths were reported by Wittig et al. (2006,
207 2007). Figure 6 shows the ϵHf - ϵNd isotope diagram for clinopyroxenes from xenoliths
208 from the northern and southern domains of the region. Those from the southern domain
209 show **relatively** little variation in ϵHf , ranging from +5.4 to +22; ϵNd values range from
210 +0.08 to +16. In contrast, samples from the northern domain show extreme values of
211 both ϵHf (+140 to +2586) and ϵNd (+2 to +91).

212 The northern Massif Central xenoliths are also very different in their isotopic
213 composition from other spinel peridotite xenoliths worldwide, as shown in Figure 7 (in
214 which the samples from the Massif Central with the highest ϵHf and ϵNd values have
215 been omitted, in order for the remaining data to be shown clearly on the scale).
216 Clinopyroxenes from almost all other mantle spinel peridotites cluster in a small area of
217 the ϵNd - ϵHf diagram (Fig. 7), near the values for Mid-Ocean Ridge Basalts and Ocean
218 Island Basalts, whereas those from the northern Massif Central show much higher ϵHf
219 values (and, more rarely, higher ϵNd values). Only a few samples (e.g. one each from
220 Lherz, Jordan and Spitsbergen) show such highly radiogenic Hf isotope values. **Such**
221 **ultradepleted lithospheric mantle domains have been discussed by Rampone and**
222 **Hofmann (2012) and Stracke et al (2011). These studies showed ϵHf values up to +110**
223 **for these depleted domains, which are low compared with those found in Massif Central**
224 **mantle clinopyroxenes ($\epsilon\text{Hf} = +140$ to +2586).**

225 $^{176}\text{Hf}/^{177}\text{Hf}$ - $^{176}\text{Lu}/^{177}\text{Hf}$ data for clinopyroxenes **from several** different mantle
226 xenoliths from the northern Massif Central (Wittig et al., 2006) form a strong
227 correlation (Fig. 8) which has been interpreted as an errorchron with an apparent
228 age of 344 ± 11 Ma. Disregarding the two samples with highest values of $^{176}\text{Hf}/^{177}\text{Hf}$ -
229 $^{176}\text{Lu}/^{177}\text{Hf}$ still yields an age of 350 ± 61 Ma. In contrast, mantle peridotites from
230 elsewhere in the world (Schmidberger et al., 2002; Le Roux et al., 2009; Choi et al.,
231 2010) all plot at the extremely low end of this array, as do the mantle garnet data of
232 Lazarov et al (2009). Even the sub-calcic garnet data for garnet peridotite xenoliths
233 from South Africa (Shu et al., 2013) plot in the low end of the array, but because of
234 the age of these garnets, their $^{176}\text{Hf}/^{177}\text{Hf}$ show a much higher dispersity than other

235 data and can therefore generate meaningful errorchrons. Thus, clinopyroxenes from
236 spinel peridotite xenoliths from the northern part of the French Massif Central are
237 much more amenable to Lu-Hf dating than those from many other regions of
238 shallow sub-continental lithospheric mantle. Clinopyroxenes from mantle xenoliths
239 from SW Poland may also be potential candidates for **future** Lu-Hf dating.

240

241 **5. DISCUSSION**

242 Extreme depletion in Hf and Zr in mantle xenoliths and their constituent clinopyroxenes
243 from the northern part of the French Massif Central was earlier reported by Lenoir et al.
244 (2000) and Downes et al. (2003). Our new LA-ICPMS analyses of clinopyroxenes
245 confirm this anomaly and also confirm the presence of strong negative anomalies in Zr
246 and Hf relative to the adjacent REE Sm and Nd in clinopyroxenes from mantle xenoliths
247 from the Polish Sudetes (Figs. 2 and 3). Few other sub-continental mantle xenolith suites
248 show this feature; those which do include some from southern Italy, western USA and
249 southern Siberia. The extreme depletion in Hf and Zr is due to a process that
250 removes these elements from the mantle, and the most obvious process is extensive
251 partial melting. Wittig et al. (2006) modeled Hf depletion in clinopyroxenes in
252 Massif Central peridotites as being due to extensive partial melting (e.g. up to 30%)
253 in the spinel peridotite stability field. **As shown in Figures 2-4, similar extreme Hf**
254 **depletion of mantle clinopyroxenes has been reported for a mantle xenoliths from**
255 **Avacha volcano, Kamchatka (Halama et al 2009).**

256 One possible origin of this extensive mantle depletion may be related to supra-
257 subduction zone processes. Since the volcanic fields of the northern Massif Central
258 and the Polish Sudetes are all situated on the northern margin of the Variscan
259 orogen, it is possible that the mantle beneath these regions experienced a similar
260 extreme depletion event, which may require two-stage melting such as is found in
261 the mantle wedge above a subducting slab. **The Hf-depleted mantle clinopyroxene**
262 **from Avacha volcano comes from a subduction setting (Halama et al., 2009).** Tok
263 (SE Siberia) and the Bearpaw Mountains (Montana) are in cratonic settings but are

264 situated above regions of recent deep subduction, which may have been the cause of
265 extreme depletion due to partial melting. Both Monte Vulture and Sicily are near to
266 subduction zones, and the mantle beneath these regions may also have experienced
267 strong depletion in this tectonic setting. However, the reason why such extensive
268 melting has only occurred in some parts of the continental lithosphere is not entirely
269 clear.

270 Comparison of the highly incompatible trace elements in mantle peridotite
271 clinopyroxenes from the northern Massif Central and SW Poland (Figures 2 and 3)
272 suggests that the lithospheric mantle beneath the two regions experienced different
273 enrichment processes. In the northern Massif Central, clinopyroxenes show relative
274 enrichment in U, La, Pb and Sr, compared to adjacent elements in their mantle-
275 normalised patterns. Mantle-normalised Nb concentrations (Nb_n) are usually lower than
276 Ta_n values; mantle-normalised Zr_n values are less than Hf_n values. In contrast, the Polish
277 mantle peridotite xenoliths have clinopyroxenes that are relatively enriched in Nb (Fig.
278 3), with mantle-normalised Nb_n always greater than Ta_n , and with many showing
279 enrichment in Zr relative to Hf. Unusually, Pb shows a relative depletion compared with
280 the adjacent REE.

281 The contrasting trace element signatures of Zr-Hf depleted clinopyroxenes in the
282 xenoliths from France and Poland are probably derived from contrasting metasomatic
283 fluids. Among the northern Massif Central xenoliths, the enrichment in fluid-mobile
284 elements such as U, Pb and Sr, and lack of enrichment in fluid-immobile ones, suggests
285 that a subduction-related fluid may have been responsible. The lack of enrichment in Zr
286 relative to Hf also implies that the fluid carried little or no Zr. Although both Lenoir et al.
287 (2000) and Wittig et al. (2006) suggested that the metasomatic agent in these xenoliths
288 might be a mantle-derived carbonatite magma, a subduction-related fluid, enriched in U,
289 Pb, Sr and LREE, is also possible.

290 In contrast, the Polish xenoliths show enrichment in both LREE and the immobile
291 elements (Zr, Nb), and additionally many of them have Zr_n greater than Hf_n , suggesting
292 that the metasomatic agent carried some Zr. This may be the result of metasomatism by

293 an alkaline silicate melt, which can carry such high-field strength elements. Again this is
294 in contrast to the earlier suggestion (Blusztajn and Shimizu 1994) that carbonatite
295 metasomatism had affected these samples. Zr-Hf depleted mantle clinopyroxenes from
296 spinel peridotites from elsewhere in the world (Figure 4) tend to resemble those from
297 Poland in terms of their enrichment in Zr relative to Hf, and the presence of Pb troughs,
298 suggesting that they have also experienced silicate melt metasomatism to some extent.

299 Significantly, in the Polish xenoliths, the Zr_n values are less than Hf_n only in those
300 samples which show lowest overall values of Zr_n and Hf_n , i.e. the most depleted
301 samples (Fig. 3). In the less depleted samples, Zr_n is greater than Hf_n , indicating that
302 Zr has been added to the clinopyroxenes after the original depletion had occurred. In
303 contrast, in the northern Massif Central samples, Zr_n is generally less than Hf_n , for
304 all samples, so there is no evidence of addition of Zr to the clinopyroxenes after the
305 initial loss of both Zr and Hf by partial melting.

306 Figure 5 shows that only a few mantle peridotites worldwide display a trend towards
307 high Lu/Hf ratios and low Hf contents in their clinopyroxenes. Other xenoliths have
308 clinopyroxene compositions that cluster around Lu/Hf ratios between 0.1 and 1.0, and
309 some suites show very little dispersion of Lu/Hf ratios. The trend shown by the
310 clinopyroxene trace element data on Figure 5 is almost certainly due to removal of
311 Hf relative to Lu, during partial melting of the mantle, since Hf is more
312 incompatible than Lu in the shallow mantle. Another possible reason for Lu-Hf
313 fractionation may be the earlier presence of garnet in the region of the mantle now
314 represented by the spinel peridotite xenoliths (i.e. garnet became unstable because
315 of a decrease in pressure perhaps by rifting or mantle uplift). Evidence for this may
316 be present as vermicular spinel-pyroxene clusters described in Northern Massif
317 Central xenoliths by Lenoir et al (2000) and Downes et al. (2003), which are
318 commonly considered to be relics of pre-existing garnet.

319 Over geological time these high Lu/Hf ratios will lead to extremely radiogenic ϵHf
320 values. In the example of the northern French Massif Central (Fig. 6), such
321 xenoliths show highly radiogenic Hf isotope ratios (ϵHf values up to +2600). Thus,

322 as shown in Fig. 7, in the northern Massif Central ϵ_{Hf} values in clinopyroxenes
323 from mantle peridotite xenoliths are much more strongly decoupled from ϵ_{Nd} values
324 compared with, for example, xenoliths from the oceanic lithosphere (e.g., Hawaii)
325 or other regions of the sub-continental lithospheric mantle (e.g. the Lherz massif in
326 the French Pyrenees; Le Roux et al., 2009). They appear to be extreme examples of
327 spinel peridotite mantle with highly radiogenic Hf isotopes. Only rare xenoliths
328 from Jordan and one from Hawaii show ϵ_{Hf} values greater than 100, although
329 unpublished data for mantle samples from Beni Bousera and Kaapvaal appear to
330 have similarly extreme values (Pearson et al., 2003).

331 Clinopyroxenes with high Lu/Hf ratios from the northern Massif Central (Wittig et
332 al., 2006) yield Hf model ages and $^{176}\text{Hf}/^{177}\text{Hf}$ - $^{176}\text{Lu}/^{177}\text{Hf}$ systematics that appear to
333 indicate that an event occurred in the mantle beneath this region in Variscan times
334 (Fig. 8). A fundamental problem with dating mantle samples is to know what
335 exactly is being dated. It is not clear whether the apparent Variscan age given by the
336 Lu-Hf systematics of Massif Central mantle clinopyroxenes actually dates a specific
337 event (e.g. depletion of Hf relative to Lu due to extensive melting). It might instead
338 date the time at which the mantle passed through the closure temperature of Lu-Hf
339 in clinopyroxene, although this temperature is not well constrained.

340 Other attempts at using Lu-Hf isotopes to date mantle events (e.g. Schmidberger et
341 al., 2002; Choi et al., 2010) have been based on much smaller variations in
342 $^{176}\text{Hf}/^{177}\text{Hf}$ - $^{176}\text{Lu}/^{177}\text{Hf}$ ratios (Fig. 8) that are unlikely to yield meaningful results
343 unless the event being dated is very old. One possible approach may be to use
344 orthopyroxene mineral separates as well as clinopyroxene as, although
345 orthopyroxene generally contains much less Hf than clinopyroxene (by an order of
346 magnitude according to Dobosi et al (2010)), the modal abundance of orthopyroxene
347 in spinel peridotites is often 2-3 times that of clinopyroxene, so a significant
348 fraction of the Hf in the rock will reside within the orthopyroxene component.
349 Mantle orthopyroxenes often show positive Zr and Hf anomalies compared to
350 adjacent elements; indeed, orthopyroxene from northern Massif Central samples
351 Mb8 and Mb57 show positive Hf anomalies, but the Hf abundance in the

352 orthopyroxene is an order of magnitude less than that in the coexisting
353 clinopyroxene (J. Puziewicz and M. Matusiak-Malek, pers. comm. 2013). Data
354 presented by Dobosi et al. (2010) show that the Lu/Hf ratio in mantle peridotite
355 orthopyroxene usually exceeds that of coexisting clinopyroxene by a factor of ~2.
356 Thus it may be possible to use orthopyroxene to extend the Lu-Hf isochron,
357 although analyzing the low levels of Hf in orthopyroxene may present technical
358 problems.

359

360 **6. CONCLUSIONS**

361 The use of the Lu-Hf system for dating events in the shallow (spinel peridotite)
362 lithospheric mantle is constrained by the behaviour of Lu and Hf during melting and
363 metasomatism. Lu concentrations in mantle clinopyroxenes tend not to vary greatly,
364 whereas Hf concentrations show wider variations as a result of depletion by partial
365 melting. Thus the variation in Lu/Hf within mantle clinopyroxenes will govern the
366 usefulness of the system to geochronology. Only a few rare peridotites show appropriate
367 depletion in Hf compared with Lu in their clinopyroxenes. Among these, the example
368 from the xenoliths from the northern part of the French Massif Central yields a
369 geologically meaningful age of 350 Ma, attributed to depletion during Variscan
370 subduction. These samples have not experienced addition of Hf during subsequent
371 metasomatism, probably because the subduction-related metasomatic fluids that affected
372 them carried little Hf. Other regions of central Europe, e.g. Lower Silesia (Poland) and
373 the Bohemian Massif (Czech Republic), have mantle xenoliths which show Hf-depletion,
374 but they have experienced later addition of Zr (and therefore perhaps Hf) during
375 metasomatism and therefore may be less likely to produce meaningful Lu-Hf model ages
376 or errorochrons.

377

378 **Acknowledgements**

379 We thank Andy Beard, Andy Carter and Martin Rittner (all at Birkbeck) for help with the
380 ICP-MS analyses, Jacek Puziewicz and Magda Matusiak-Malek (Wroclaw, Poland) for

381 additional LA-ICPMS determinations, and Jerzy Blusztajn (WHOI) for providing the
382 samples from Poland. We appreciate the constructive comments on this manuscript from
383 Elis Hoffmann, Ralf Halama, Sonja Aulbach, Sebastian Tappe, Theo Ntaflos, Dimitri
384 Ionov and Laurie Reisberg.

385

386 **References**

387 Ackerman L, Medaris G, Spacek P and Ulrych J 2014. Geochemical and petrological
388 constraints on mantle composition of the Ohre (Eger) rift, Bohemian Massif:
389 peridotite xenoliths from the Ceske Stredohori volcanic complex and northern
390 Bohemia. *Int. J. Earth Sci.* in press.

391 Arai S and Ishimaru S 2008. Insights into petrological characteristics of the
392 lithosphere of mantle wedge beneath arcs through peridotite xenoliths: a review. *J*
393 *Petrol.* 49, 665-695.

394 Aulbach S, Griffin W L, O'Reilly S Y and McCandless T E 2004. Genesis and
395 evolution of the lithospheric mantle beneath the Buffalo Head Terrane, Alberta
396 (Canada). *Lithos* 77, 413-451.

397 Babuska V, Plomerova J and Vecsey L., 2002. Seismic anisotropy of the French Massif
398 Central and predisposition of Cenozoic rifting and volcanism by Variscan suture hidden
399 in the mantle lithosphere. *Tectonics* 21, 1-20.

400 Bianchini G, Beccaluva L, Bonadiman C, Nowell G, Pearson G, Siena F and Wilson M
401 2007. Evidence of diverse depletion and metasomatic events in harzburgite-lherzolite
402 mantle xenoliths from the Iberian plate (Olot, NE Spain): implications for lithosphere
403 accretionary processes. *Lithos* 94, 25-45.

404 Bizimis M, Griselein M, Lassiter J C, Salters V J M and Sen G 2007. Ancient recycled
405 mantle lithosphere in the Hawaiian plume: Osmium-Hafnium isotopic evidence from
406 peridotite mantle xenoliths. *Earth Planet Sci. Lett.* 257, 259-273.

407 Blusztajn J and Shimizu N, 1994. The trace element variations in clinopyroxenes from
408 spinel peridotite xenoliths from southwest Poland. *Chem. Geol.* 111, 227-243.

409 Bonadiman C, Coltorti M, Duggen S, Paludetti L, Siena F, Thirlwall M F and Upton B
410 G J 2008. Palaeozoic subduction related and kimberlite or carbonatite metasomatism
411 in the Scottish lithospheric mantle. In: Coltorti M and Gregoire M (eds).
412 *Metasomatism in Oceanic and Continental Lithospheric Mantle.* Geol. Soc. Lond. Sp.
413 Pub. 293, 303-333.

- 414 Choi S H, Suzuki K, Mukasa S B, Lee J-I and Jung H, 2010. Lu-Hf and Re-Os
415 systematics of peridotite xenoliths from Spitsbergen, western Svalbard: implications
416 for mantle-crust coupling. *Earth Planet. Sci. Lett.* 297, 121-132.
- 417 Deng, F.L. and McDougall, J.D., 1992. Proterozoic depletion of the lithosphere recorded
418 in mantle xenoliths from Inner Mongolia. *Nature*, 360: 333-336.
- 419
420 Dobosi G, Jenner G A, Embey-Isztin A and Downes H 2010. Cryptic metasomatism in
421 clino- and orthopyroxene in the upper mantle beneath the Pannonian region. In:
422 *Petrological Evolution of the European Lithospheric Mantle*. Geol. Soc. London. Sp.
423 Pub. 337, 177-194.
- 424 Downes H, Kostoula T, Jones A, Beard A, Thirlwall M and Bodinier J-L 2002.
425 Geochemistry and Sr-Nd isotopic compositions of mantle xenoliths from the Monte
426 Vulture carbonatite-melilitite volcano, central southern Italy. *Contrib. Mineral. Petrol.*
427 144, 78-92.
- 428 Downes H, Reichow M K, Mason P R D, Beard A D and Thirlwall M F 2003. Mantle
429 domains in the lithosphere beneath the French Massif Central: trace element and isotopic
430 evidence from mantle clinopyroxenes. *Chemical Geology* 200, 71-87.
- 431 Downes, H., Macdonald, R., Upton, B.G.J., Cox, K.G., Bodinier, J-L., Mason,
432 P.R.D., James, D., Hill, P.G. and Hearn.B.C. Jr. 2004. Ultramafic xenoliths from the
433 Bearpaw Mountains, Montana, USA: Evidence for multiple metasomatic events in
434 the lithospheric mantle beneath the Wyoming Craton. *Journal of Petrology* 45, 1631-
435 1662.
- 436 Femenias O, Coussaert N, Bingen B, Whitehouse M, Mercier J-C C and Demaiffe D
437 2003. A Permian underplating event in late- to post-orogenic tectonic setting. Evidence
438 from the mafic-ultramafic layered xenoliths from Beaunit (French Massif Central).
439 *Chem. Geol.* 199, 293-315.
- 440 Gonzaga R G, Menzies M A, Thirlwall M F, Jacob D E and LeRoex A 2010. Eclogites
441 and garnet pyroxenites: Problems resolving provenance using Lu-Hf, Sm-Nd and Rb-Sr
442 isotope systems. *J. Petrology* 51, 513-535.
- 443 Gregoire M, Tinguely C, Bell D R and le Roex A P 2005. Spinel lherzolite xenoliths
444 from the Premier kimberlite (Kapaal craton, South Africa): Nature and evolution of
445 the shallow upper mantle beneath the Bushveld complex. *Lithos* 84, 185-205.
- 446 Halama R, Savov I P, Rudnick R L, McDonough W F 2009. Insights into Li and Li
447 isotope cycling and sub-arc metasomatism from veined mantle xenoliths, Kamchatka.
448 *Contrib. Mineral. Petrol.* 158, 197-222.
- 449 Handler, M.R., Wysoczanski, R.J. and Gamble, J.A., 2003. Proterozoic lithosphere in
450 Marie Byrd Land, West Antarctica: Re-Os systematics of spinel peridotite xenoliths.
451 *Chemical Geology*, 196: 131-145.

452 Ionov D A 2004. Chemical variations in peridotite xenoliths from Vitim, Siberia:
453 Inferences for REE and Hf-behaviour in the garnet-facies upper mantle. *J Petrol.* 45,
454 343-367.

455 Ionov D A, Chazot G, Chauvel C, Merlet C, Bodinier J L 2006a. Trace element
456 distribution in peridotite xenoliths from Tok, SE Siberian craton: A record of pervasive
457 multi-stage metasomatism in the shallow refractory mantle. *Geochim. Cosmochim.*
458 *Acta* 70, 1231-1260.

459 Ionov D A, Shirey S B, Weiss D and Brugmann G 2006b. Os-Hf-Sr-Nd isotope and
460 PGE systematics of spinel peridotite xenoliths from Tok, SE Siberian craton: Effects of
461 pervasive metasomatism in the shallow refractory mantle. *Earth Planet. Sci. Lett.* 241,
462 47-64.

463 Ishimaru S, Arai S, Ishida Y, Shirasaka M, and Okrugin M, 2007. Melting and multi-
464 stage metasomatism in the mantle wedge beneath a frontal arc inferred from highly
465 depleted peridotites xenoliths from the Avacha volcano, southern Kamchatka. *J. Petrol.*
466 48, 395-433.

467 Janney P E, Shirey S B, Carlson R W, Pearson D G, Bell D R, Le Roex A P, Ishikawa
468 A, Nixon P H and Boyd F R 2010. Age, composition and thermal characteristics of
469 South African off-craton mantle lithosphere: evidence for a multi-stage history. *J.*
470 *petrology*, 51, 1849-1890.

471 Lazarov M, Brey G P and Weyer S 2009. Time steps of depletion and enrichment in the
472 Kaapvaal craton as recorded by subcalcic garnets from Finsch (SA). *Earth Planet. Sci.*
473 *lett* 279, 1-10.

474 Lenoir X, Garrido C J, Bodinier J and Dautria J 2000. Contrasting lithospheric mantle
475 domains beneath the Massif Central (France) revealed by geochemistry of peridotite
476 xenoliths. *Earth Planet. Sci. Lett.* 181, 359-375.

477 Le Roux V, Bodinier J-L, Alard O, S Y and Griffin W L 2009. Isotopic decoupling of
478 Hf, Nd and Sr during porous melt flow: a case study in the Lherz peridotites (Pyrenees).
479 *Earth Planet. Sci. Lett.* 279, 76-85.

480 Marks M, Halama R, Wenzel T and Markl G 2004. Trace element variations in
481 clinopyroxene and amphibole from alkaline to peralkaline syenites and granites:
482 implications for mineral-melt trace-element partitioning. *Chem. Geol.* 211, 185-215.

483 Mason P, Jarvis K E, Downes H and Vannucci R 1999. Determinations of incompatible
484 trace elements in mantle clinopyroxenes by LA-ICP-MS: a comparison of analytical
485 performance with established techniques. *J of Geostand. Geoanalysis*, 23, 157-172.

486 Matusiak-Malek, M., Puziewicz, J., Ntaflos, T., Grégoire, M. & Downes, H. 2010.
487 Metasomatic effects in the lithospheric mantle beneath the NE Bohemian Massif: A
488 case study of Lutynia (SW Poland) peridotite xenoliths. *Lithos* 117, 49-60.

- 489 McInnes B I A, Gregoire M, Binns R A, Herzig P M and Hannington M D, 2001.
490 Hydrous metasomatism of oceanic sub-arc mantle, Lihir, Papua New Guinea: petrology
491 and geochemistry of fluid-metasomatised mantle wedge xenoliths. *Earth Planet. Sci.*
492 *Lett.* 188, 169-183.
- 493 Nasir S and Rollinson H 2009. The nature of the subcontinental lithospheric mantle
494 beneath the Arabian Shield: Mantle xenoliths from southern Syria. *Precambrian*
495 *Research* 172, 323-333.
- 496 Pearson D G, Canil D and Shirey S B 2003. Mantle samples included in volcanic rocks:
497 Xenoliths and diamonds. *Treatise on Geochemistry* vol 2, Section 2.05.
- 498 Pearce N J G, Perkins W T, Westgate J A, Gorton M P, Jackson S E, Neal C R and
499 Chenery S P 1997. A compilation of new and published major and trace element data
500 for NIST SRM 610 and NIST SRM 612 glass reference standards. *Geostand. Newsletter*
501 21, 115-144.
- 502 Perinelli C, Sapienza G T, Armienti P and Morten L 2008. Metasomatism of the upper
503 mantle beneath the Hyblean Plateau (Sicily): evidence from pyroxenes and glass in
504 peridotite xenoliths. In: Coltorti M and Gregoire M (eds). *Metasomatism in Oceanic and*
505 *Continental Lithospheric Mantle*. Geol. Soc. Lond. Sp. Pub. 293, 197-221.
- 506 Puziewicz, J., Koepke, J., Grégoire, M., Ntaflos, T. & Matusiak-Malek, M. 2011.
507 Lithospheric Mantle Modification during Cenozoic Rifting in Central Europe: Evidence
508 from the Ksieginki Nephelinite (SW Poland) Xenolith Suite. *Journal of Petrology* 52,
509 2107-2145.
- 510
511 Rampone E and Hofmann A W 2012. A global overview of isotopic heterogeneities in
512 the oceanic mantle. *Lithos* 148, 247-261.
- 513
514 Rudnick, R.L. and Walker, R.J., 2009. Interpreting ages from Re–Os isotopes in
515 peridotites. *Lithos* 112 (S), 1083-1095.
- 516 Sanchez-Rodriguez L and Gebauer D 2000. Mesozoic formation of pyroxenites and
517 gabbros in the Ronda area (southern Spain), followed by early Miocene subduction
518 metamorphism and emplacement into the middle crust: U-Pb sensitive high-resolution
519 ion microprobe dating of zircon. *Tectonophysics* 316, 19-44.
- 520 Scherer E, Münker C and Mezger K., 2001. Calibration of the Lutetium-Hafnium Clock.
521 *Science* 293, 683-687.
- 522 Schmidberger S S, Simonetti A and Francis D 2001. Sr-Nd-Pb isotope systematics of
523 mantle xenoliths from Somerset Island kimberlites: Evidence for lithosphere stratification
524 beneath Arctic Canada. *Geochim. Cosmochim. Acta.* 65, 4243-4255.
- 525 Schmidberger S S, Simonetti A, Francis D and Garipey C 2002. Probing Archean
526 lithosphere using the Lu-Hf isotope systematics of peridotite xenoliths from Somerset
527 Island kimberlites, Canada. *Earth Planet. Sci. Lett.* 197, 245-259.

- 528 Schmidberger S S, Simonetti A, Heaman L M, Creaser R A and Whiteford S 2007. Lu-
529 Hf, in-situ Sr and Pb isotope and trace element systematics for mantle eclogites from the
530 Diavik diamond mine: Evidence for Palaeoproterozoic subduction beneath the Slave
531 craton, Canada. *Earth Planet. Sci. Lett.* 254, 55-68.
- 532 Schmidt, G. and Snow, J., 2002. Os isotopes in mantle xenoliths from the Eifel volcanic
533 field and the Vogelsberg (Germany): age constraints on the lithospheric mantle.
534 *Contributions to Mineralogy and Petrology*, 143: 694-705.
- 535 Shaw J E, Baker J A, Kent A J R, Ibrahim K M and Menzies M A, 2007. The
536 geochemistry of the Arabian lithospheric mantle – a source for intraplate volcanism? *J.*
537 *Petrol.* 48, 1495-1512.
- 538 Shu Q, Brey G P, Gerdes A and Hofer H 2013. Geochronological and geochemical
539 constraints on the formation and evolution of the mantle underneath the Kaapvaal craton:
540 Lu-Hf and Sm-Nd systematics of subcalcic garnets from highly depleted peridotites.
541 *Geochimica et Cosmochimica Acta* 113, 1-20.
- 542 Söderlund U, Patchett P J, Vervoort J D and Isachsen C E 2004. The ^{176}Lu decay
543 constant determined by Lu-Hf and U-Pb isotope systematics of Precambrian mafic
544 intrusions. *Earth Planet. Sci. Lett.*
- 545 Stracke A, Snow J E, Hellebrand E, von der Handt A, Bourdon B, Birbaum K and
546 Günther D, 2011. Abyssal peridotites Hf isotopes identify extreme mantle depletion.
547 *Earth Planet. Sci. Lett.* 308, 359-368.
- 548 Sun S-S and McDonough W F 1989. Chemical and isotopic systematics of ocean basalts:
549 implications for mantle composition and processes. In: Saunders A D and Norry M J
550 (Eds). *Magmatism in the Ocean Basins*. *Geol. Soc. Sp. Pub.* 42, 313-345.
- 551 Tappe S, Smart K A, Pearson D G, Steenfelt A and Simonetti A 2011. Craton formation
552 in Late Archean subduction zones revealed by first Greenland eclogites. *Geology*, 39,
553 1103-1106.
- 554 Teklay M, Scherer E, Mezger K and Danyushevsky L 2010. Geochemical characteristics
555 and Sr-Nd-Hf isotope compositions of mantle xenoliths and host basalts from Assab,
556 Eritrea: implications for the composition and thermal structure of the lithosphere beneath
557 the Afar Depression. *Contrib. Mineral. Petrol.* 159, 731-351.
- 558 Vannucci R, Ottolini L, Bottazzi P, Downes H and Dupuy C 1994. INAA, IDMS and
559 SIMS comparative REE investigations of clinopyroxenes from mantle xenoliths with
560 different textures. *Chem. Geol.* 118. 85-108.
- 561 Widom, E., Kepezhinskas, P. and Defant, M., 2003. The nature of metasomatism in the
562 sub-arc mantle wedge: evidence from Re-Os isotopes in Kamchatka peridotite xenoliths.
563 *Chemical Geology*, 196: 283-306.
564

- 565 Witt-Eickschen G and Kramm U 1997. Mantle upwelling and metasomatism beneath
566 central Europe: Geochemical and isotopic constraints from mantle xenoliths from the
567 Rhön (Germany). *J. Pet.* 38, 479-493.
- 568 Wittig N, Baker J A, Downes H 2006. Dating the mantle roots of young continental crust.
569 *Geology* 34, 237-240.
- 570 Wittig N, Baker J A, Downes H 2007. U-Th-Pb and Lu-Hf isotopic constraints on the
571 evolution of sub-continental lithospheric mantle, French Massif Central. *Geochim.*
572 *Cosmochim. Acta*, 71, 1290-1311.
- 573 Wittig N, Pearson D G, Downes H and Baker J A 2009. The U, Th and Pb elemental and
574 isotopic compositions of mantle clinopyroxenes and their grain boundary contamination
575 derived from leaching and digestion experiments. *Geochim. Cosmochim. Acta*, 73, 469-
576 488.
- 577 Wittig, N., Pearson, D.G., Baker, J.A., Duggen, S. and Hoernle, K., 2010a. A major
578 element, PGE and Re-Os isotope study of Middle Atlas (Morocco) peridotite xenoliths:
579 Evidence for coupled introduction of metasomatic sulphides and clinopyroxene. *Lithos*,
580 115: 15-26.
- 581 Wittig, N. Webb M, Pearson D G, Dale C W, Ottley C J, Hutchison M, Jensen S M and
582 Luget A., 2010b. Formation of the North Atlantic Craton: Timing and mechanisms
583 constrained from Re-Os isotope and PGE data of peridotite xenoliths from S.W.
584 Greenland. *Chemical Geology*, 276: 166-187.
- 585 Wittig N, Pearson D G, Duggen S, Baker J A and Hoernle K, 2010c. Tracing the
586 metasomatic and magmatic evolution of continental mantle roots with Sr, Nd, Hf and Pb
587 isotopes: a case study of Middle Atlas (Morocco) peridotite xenoliths. *Geochim.*
588 *Cosmochim. Acta*. 74, 1417-1435.
- 589 Xu X, Griffin W L, O'Reilly S Y, Pearson N J, Geng H and Zheng J, 2008. Re-Os
590 isotopes of sulfides in mantle xenoliths from eastern China: progressive modification of
591 the lithospheric mantle. *Lithos* 102, 43-64.
- 592 Yu J-H, O'Reilly S Y, Zhang M, Griffin W L and Xu X 2006. Roles of melting and
593 metasomatism in the formation of the lithospheric mantle beneath the Leizhou
594 peninsula, south China. *J. Pet.* 47, 355-383.
- 595 Yu S-Y, Xu Y-G, Huang X-L, Ma J-L, Ge W-C, Zhang H-H and Qin X-F 2009. Hf-Nd
596 isotopic decoupling in continental mantle lithosphere beneath Northeast China: effects
597 of pervasive mantle metasomatism. *J. Asian Earth Sci.* 35, 554-570.
- 598 Zangana N A 1995. Geochemical variations in mantle xenoliths from Ray pic, Massif
599 Central, France. Unpub. PhD thesis, University of London.
- 600 Zangana NA, Downes H, Thirlwall M F, Marriner G F and Bea F 1998. Geochemical
601 variation in peridotite xenoliths and their constituent clinopyroxenes from Ray Pic

602 (French Massif Central): implications for the composition of the shallow lithospheric
603 mantle. Chem. Geol. 153, 11-35.

604 Zheng J, Griffin W L, O'Reilly S Y, Zhang M and Pearson N, 2006. Zircons in mantle
605 xenoliths record the Triassic Yangtze-North China continental collision. Earth Planet.
606 Sci. Lett. 247, 130-142.

607

608 **Figure Captions**

609 Figure 1 Sm/Nd vs Lu/Hf ratios in clinopyroxenes from spinel peridotite mantle rocks
610 from worldwide localities. Data Sources: NFMC = North French Massif Central (Table
611 1); SFMC = South French Massif Central (Table 1); Poland (Table 2); Pannonian Basin
612 (unpublished data, CDV); Jordan (Shaw et al., 2007); China (Leizhou – Yu et al.,
613 2006); Vulture (Italy - Downes et al., 2002); Rhön (Witt-Eickschen and Kramm,
614 1997); Tok, Siberia (Ionov et al., 2006); Hawaii (Bizimis et al., 2007); Premier, South
615 Africa (Gregoire et al., 2005); Bearpaws, Montana, USA (Downes et al., 2004);
616 Morocco (Wittig et al., 2010c); NE Spain (Bianchini et al., 2007); Alberta (Aulbach et
617 al., 2004). Values for primitive mantle (Sm/Nd = 0.328; Lu/Hf = 0.239) from Sun and
618 McDonough (1989).

619 Figure 2. LA-ICPMS data for clinopyroxene in representative mantle xenoliths from
620 the Northern Massif Central compared with those of the Southern Massif Central (data
621 from Table 1), normalised to primitive mantle (Sun and McDonough 1989). Data
622 shown by grey squares and dashed line are for clinopyroxene in mantle xenoliths from
623 Avacha volcano, Kamchatka, situated above an active subduction zone (Halama et al.,
624 2009).

625 Figure 3. LA-ICPMS data for clinopyroxene in mantle xenoliths from Polish Sudetes
626 (data from Table 2) normalised to primitive mantle (Sun and McDonough 1989). Data
627 shown by grey squares and dashed line are for clinopyroxene in mantle xenoliths from
628 Avacha volcano, Kamchatka, situated above an active subduction zone (Halama et al.,
629 2009).

630 Figure 4. Zr-Hf-depleted clinopyroxenes from mantle xenoliths from Mte Vulture Italy
631 - Downes et al., 2002; Sicily - Perinelli et al., 2008; Bearpaw Mts (Wyoming - Downes
632 et al., 2004), Middle Atlas (Morocco - Wittig et al., 2010c), Tok (Siberia - Ionov et al.,
633 2006), Plesny (Bohemian massif - Ackerman et al., in press), normalised to primitive
634 mantle (Sun and McDonough 1989). Data shown by grey squares and dashed line are
635 for clinopyroxene in mantle xenoliths from Avacha volcano, Kamchatka, situated
636 above an active subduction zone (Halama et al., 2009).

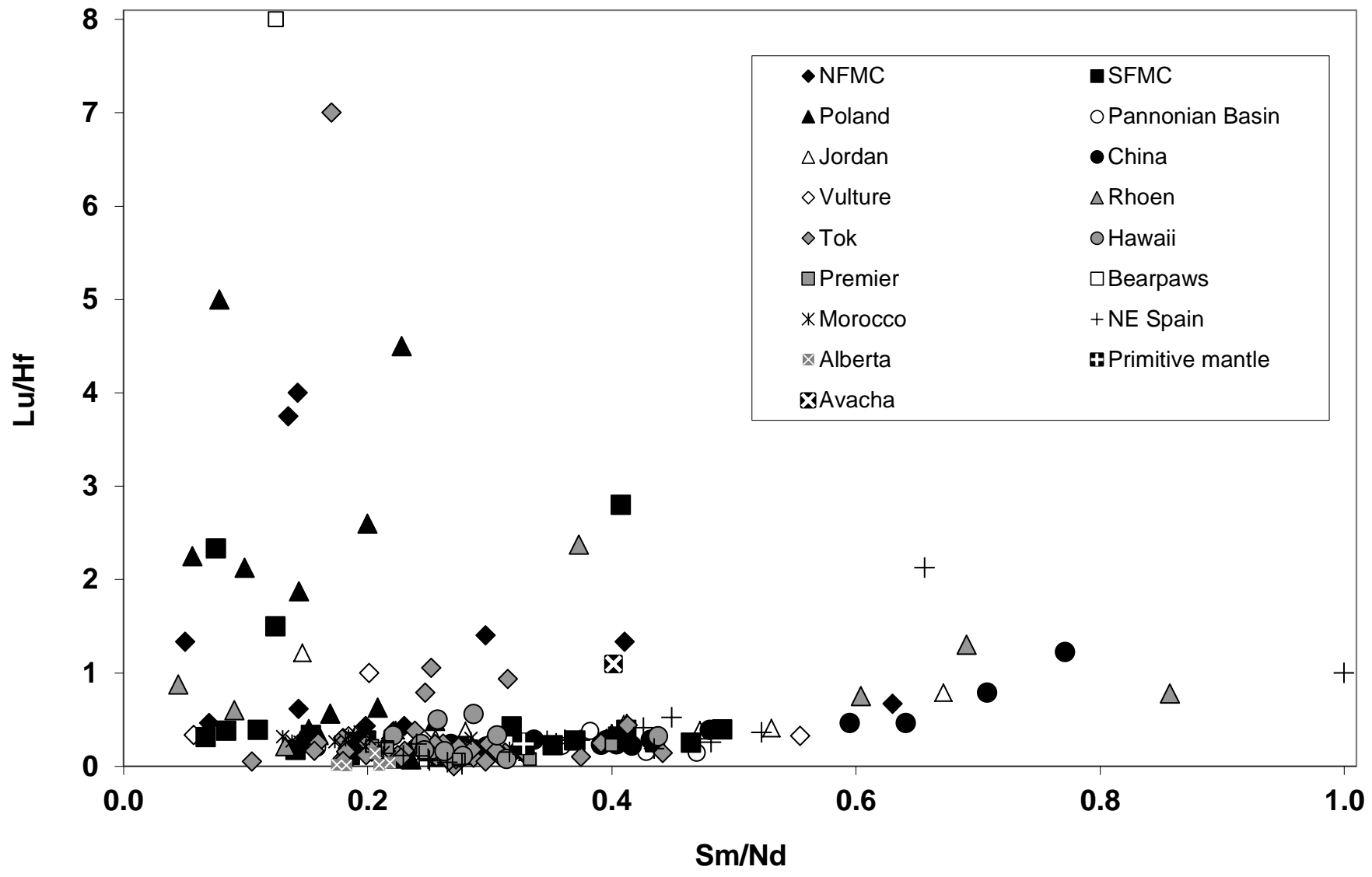
637 Figure 5. Lu/Hf ratio vs Hf concentration (ppm) in clinopyroxenes from mantle spinel
638 peridotite xenoliths worldwide. Data sources as for Fig. 1. Note logarithmic scales on
639 both axes. A few show extreme Hf-depletion and consequent high Lu/Hf ratios similar
640 to those of the Southern French Massif Central. Arrow indicates increasing extent of
641 partial melting. Values for primitive mantle from Sun and McDonough (1989). Data

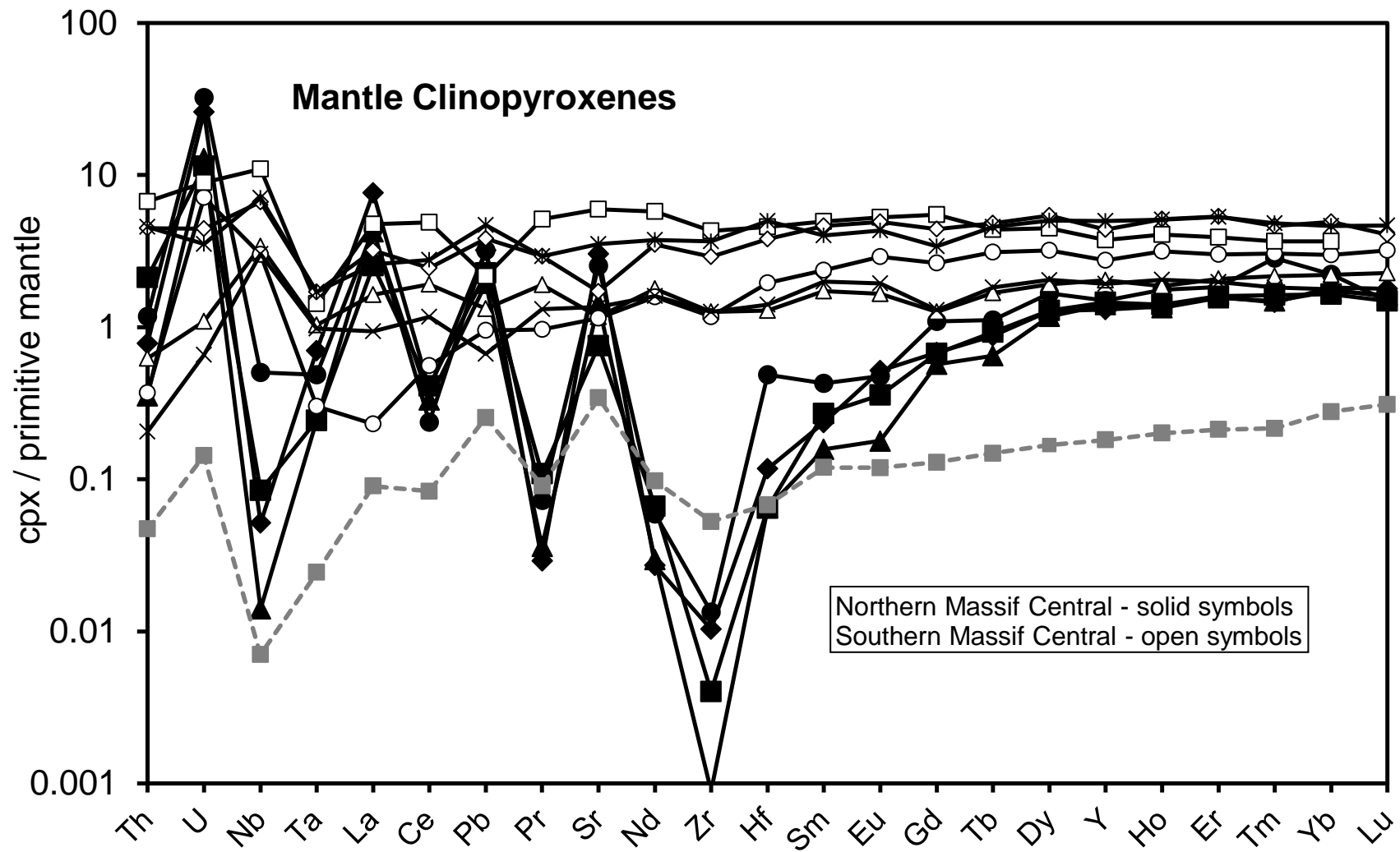
642 shown by grey squares and dashed line are for clinopyroxene in mantle xenoliths from
643 Avacha volcano, Kamchatka, situated above an active subduction zone (Halama et al.,
644 2009).

645 Figure 6. ϵHf - ϵNd isotope data for clinopyroxenes from mantle spinel peridotite
646 xenoliths from French Massif Central showing differences between northern and
647 southern regions (Wittig et al., 2007). Inset shows expanded field of southern Massif
648 Central samples compared with the field for Mid-Ocean Ridge Basalts and Ocean
649 Island Basalts (dashed line).

650 Figure 7. ϵHf - ϵNd isotope data for clinopyroxenes from mantle peridotites worldwide
651 (data sources as follows: Jordan – Shaw et al., 2007; Alberta – Aulbach et al., 2004;
652 Hawaii – Bizmis et al., 2007; Tok – Ionov et al., 2006b; Somerset Island (Canada) –
653 Schmidberger et al., 2001, 2002; Scotland – Bonadiman et al., 2008; Olot (Spain) –
654 Bianchini et al., 2007; Middle Atlas (Morocco) – Wittig et al., 2010c; Eritrea – Teklay et
655 al., 2010; NE China – Yu et al., 2009; Spitsbergen – Choi et al., 2010; Lherz massif –
656 Le Roux et al., 2009; Gakkel Ridge – Stracke et al., 2011), compared with ϵHf - ϵNd
657 isotope data from clinopyroxenes from the northern Massif Central peridotite xenoliths
658 (Wittig et al., 2007). The most enriched compositions from the northern Massif Central
659 shown on Figure 6 have been omitted.

660 Figure 8. Lu-Hf isochron diagram for clinopyroxenes from spinel peridotite mantle
661 xenoliths from the northern Massif Central, showing a reference isochron of 344 ± 11 Ma
662 (Wittig et al., 2006), compared to data from other regions of sub-continental
663 lithospheric mantle (Schmidberger et al., 2002; Le Roux et al., 2009; Choi et al., 2010).
664 Inset shows the reference isochron of 350 ± 61 Ma for the northern Massif Central
665 samples minus the two with the highest Lu/Hf ratios.





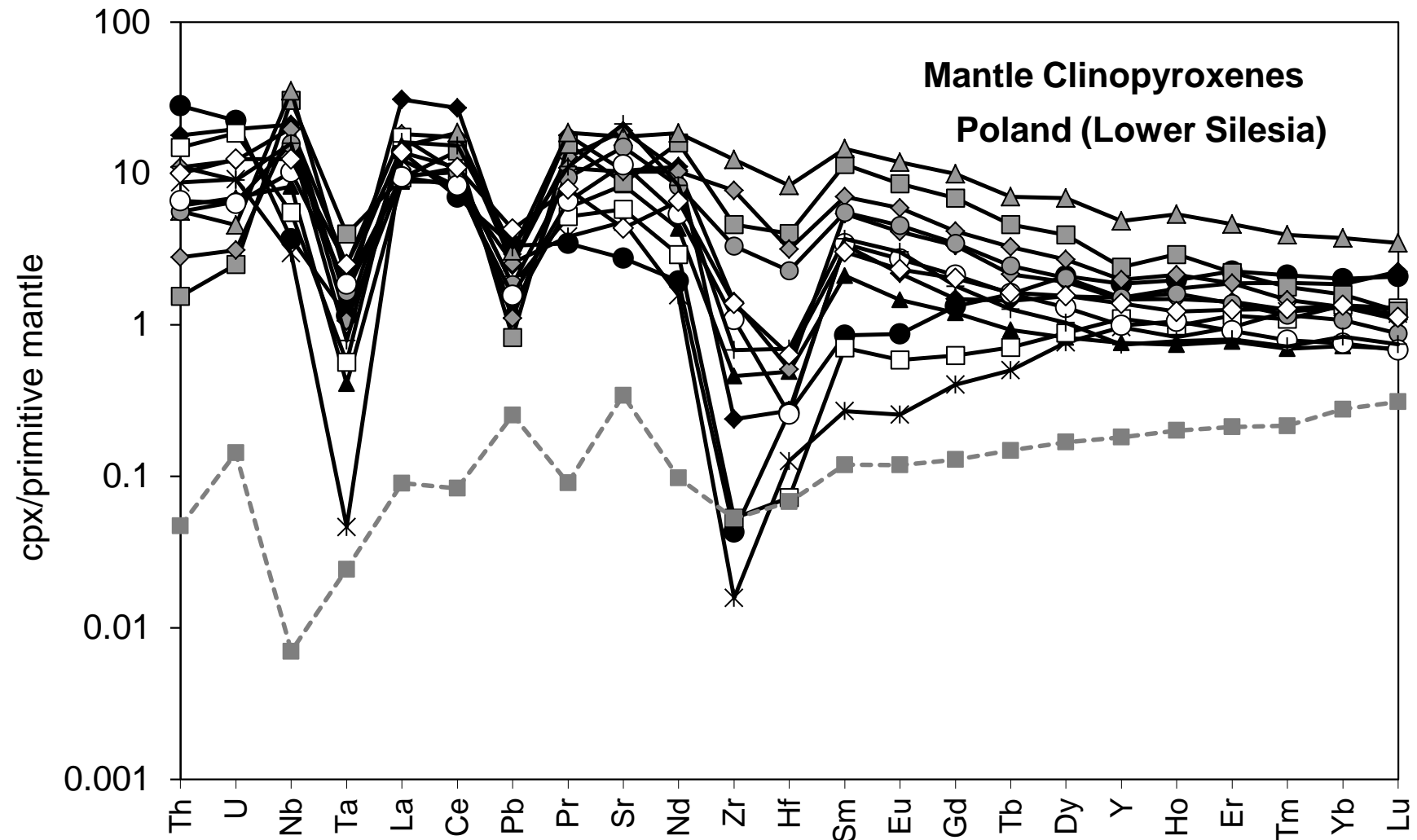
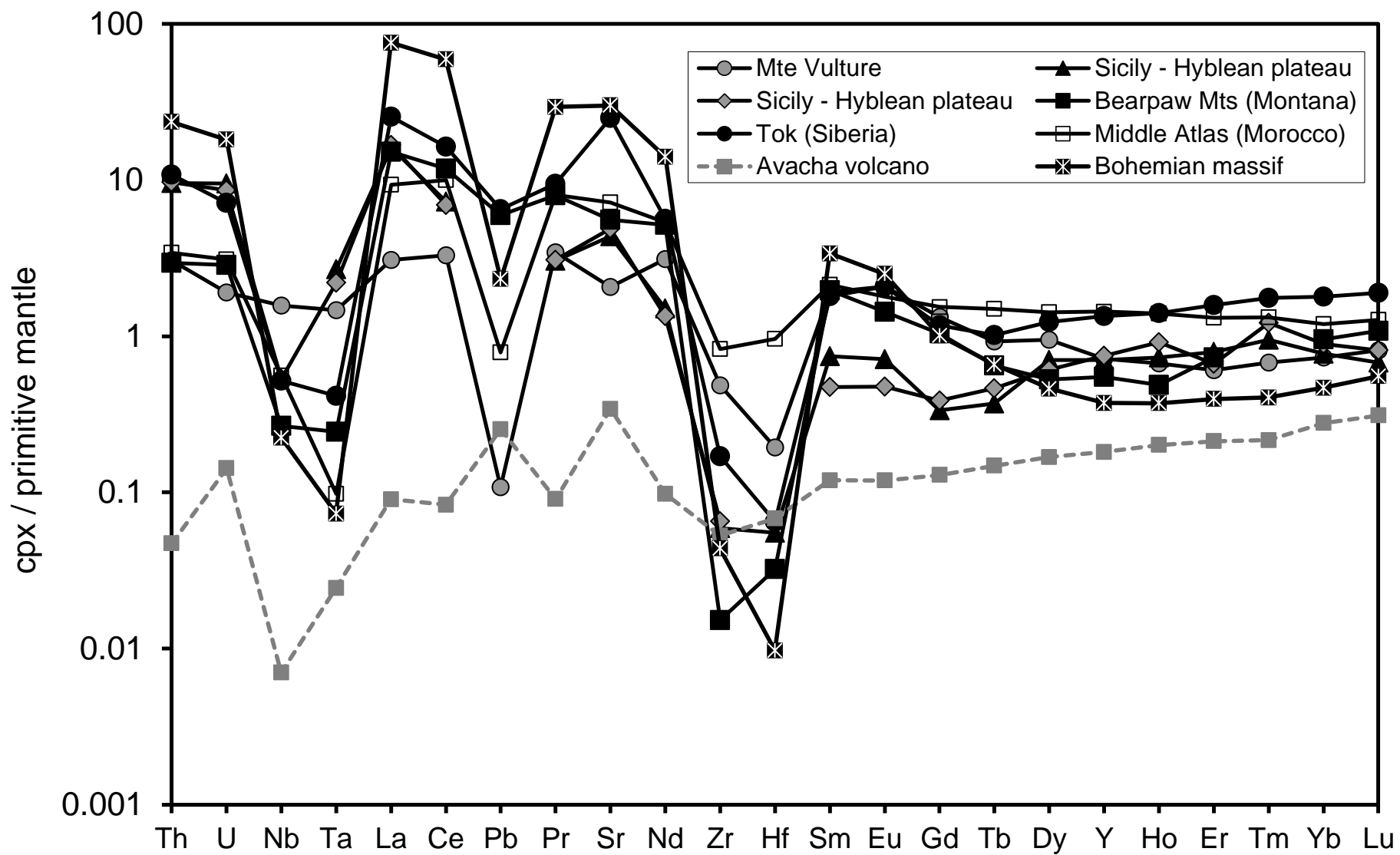
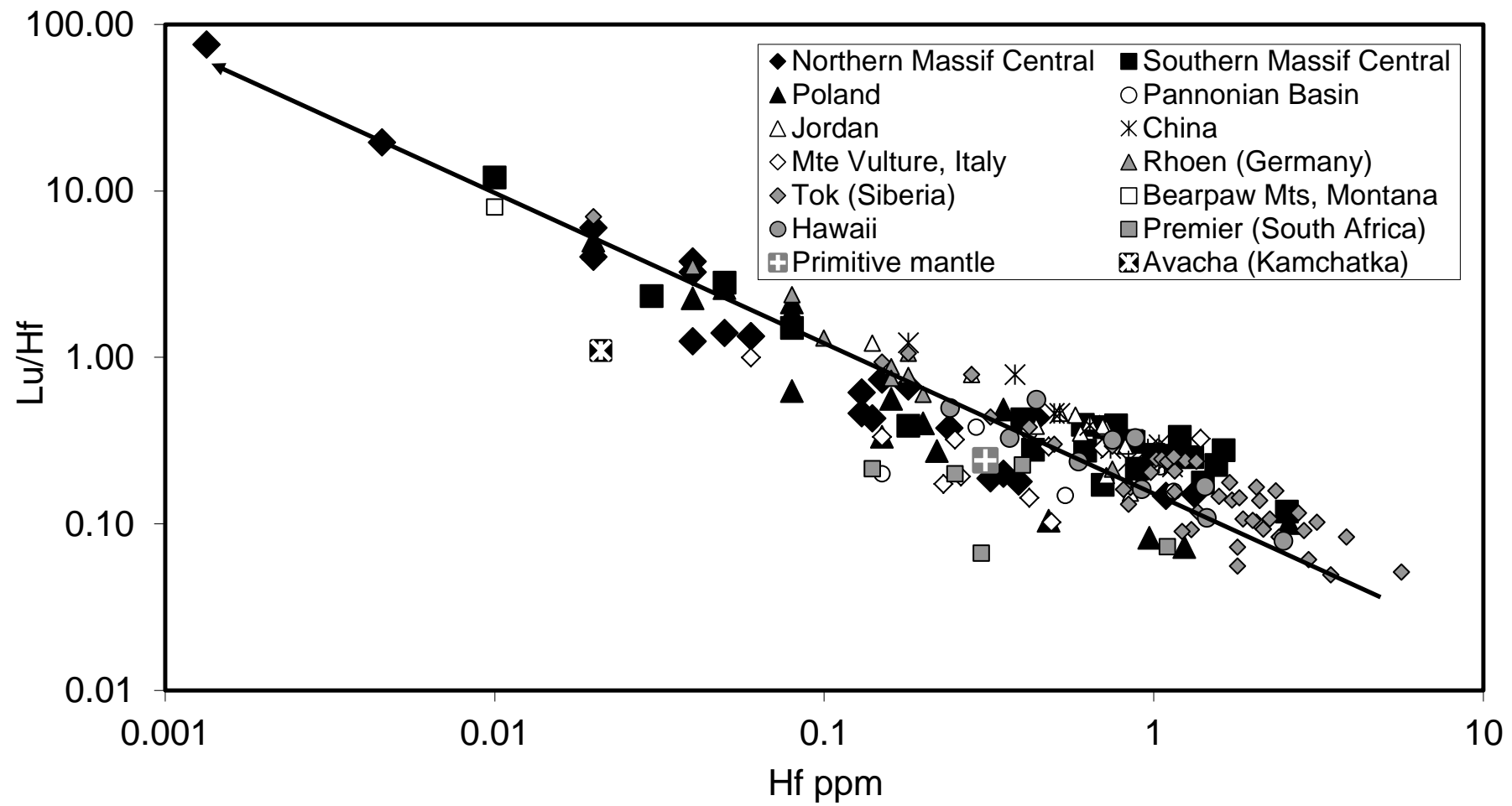


Figure
[Click here to download Figure: Fig 4 other cpx.pdf](#)





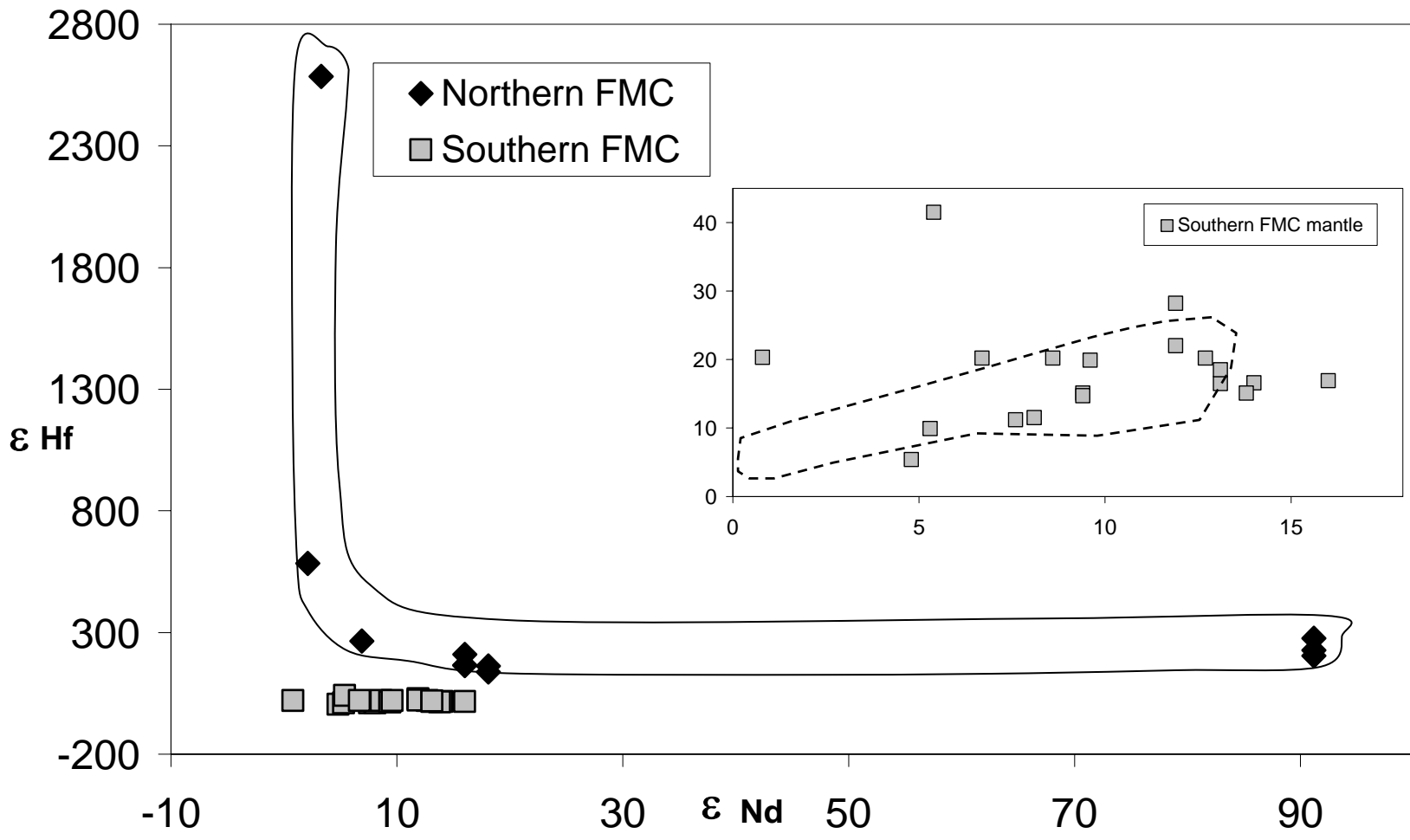


Figure
[Click here to download Figure: Fig 7 Nd-Hf isotopes.pdf](#)

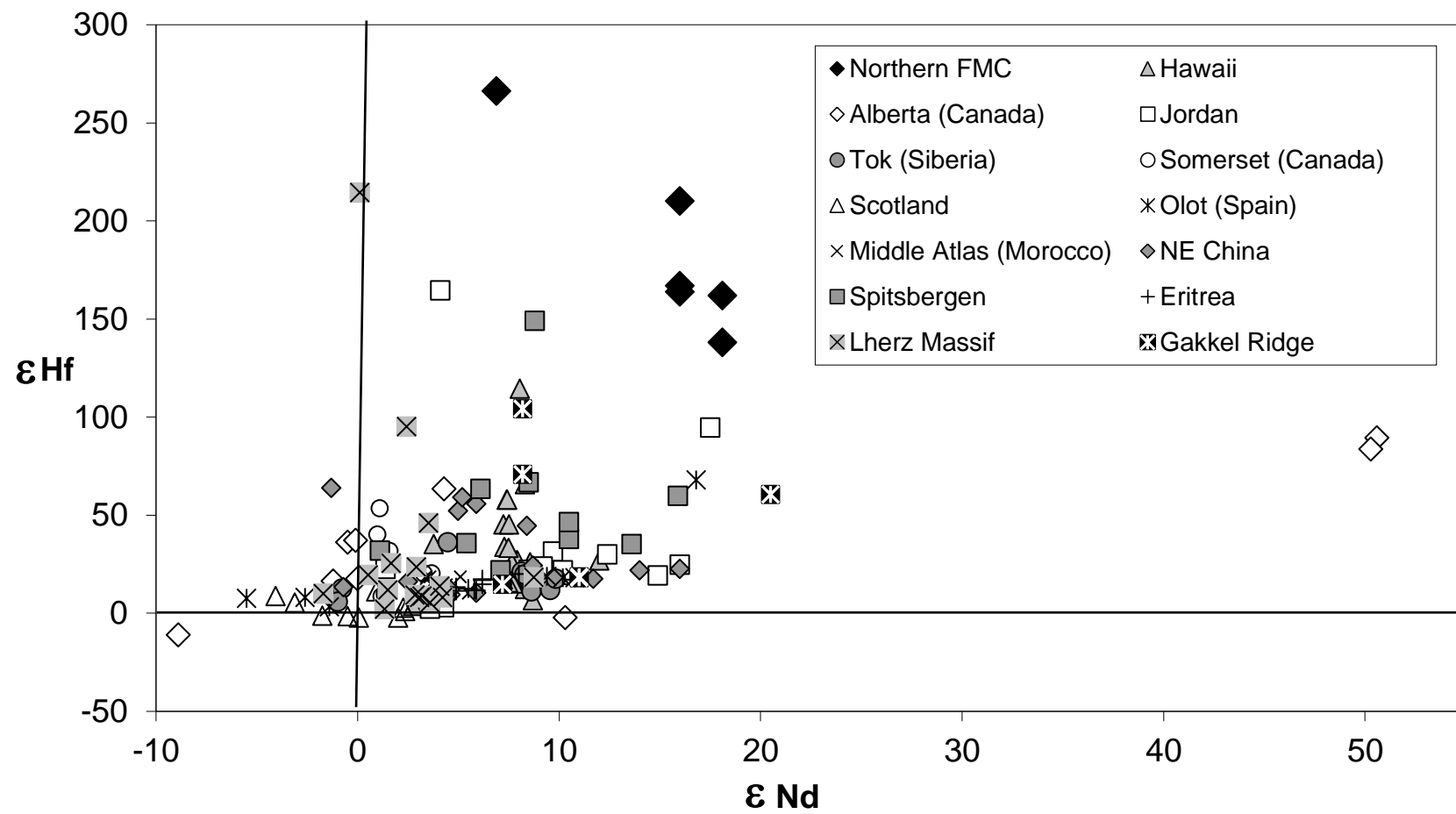


Figure
[Click here to download Figure: Figure 8 isochron.pdf](#)

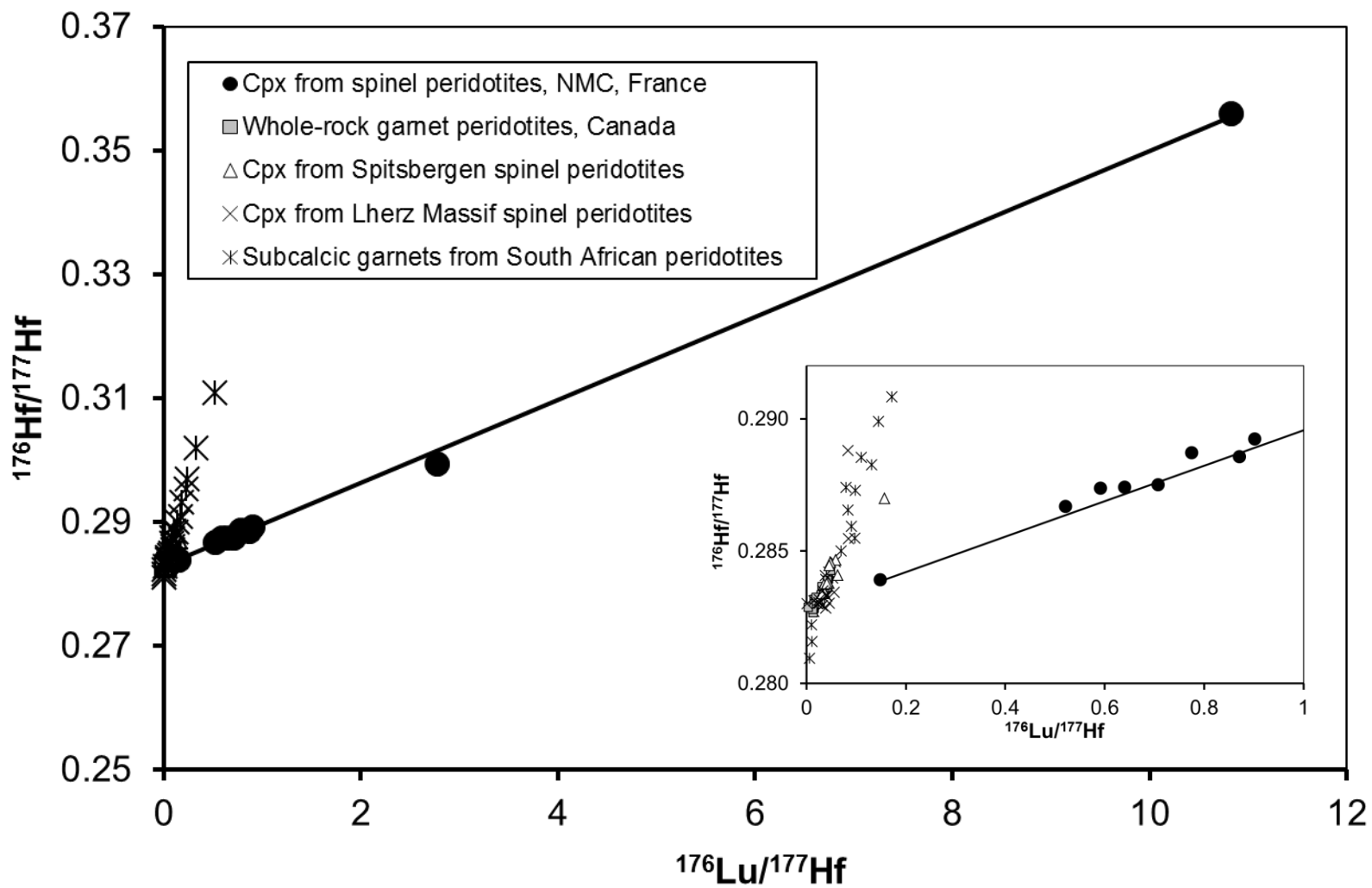


Table 1. Analyses of clinopyroxenes from French Massif Central, by LA-ICP-MS. NMC = Northern Domain

element	RP83-72 SMC	RP87-2 SMC	RP91-20 SMC	BO83-74 SMC	Ta 7 SMC	Ta 13 SMC	Ta 19 SMC	Gr83-75 SMC
Rb				0.01		0.03	0.02	0.02
Ba				0.05		0.31	0.27	0.09
Th	2.80	0.02	0.02	0.02	0.90	0.56	0.74	0.05
U	0.51	0.02	0.02	0.01	0.24	0.27	0.21	0.02
Nb	0.15	0.05	0.08	2.17	0.70	8.86	7.49	2.42
Ta	0.03	0.02	0.02	0.04	0.02	0.01	0.09	0.04
La	20.00	0.34	0.12	0.65	6.70	1.84	11.42	1.12
Ce	58.00	2.35	1.11	2.08	7.20	5.69	19.67	3.39
Pb	0.67	0.18	0.70	0.12	1.20	0.49	0.31	0.24
Pr	6.70	0.62	0.34	0.36	0.90	0.68	2.78	0.53
Sr	353.0	49.0	24.0	28.7	103.0	55.7	240.4	24.7
Nd	22.00	3.61	2.50	2.17	4.30	8.86	7.49	2.42
Zr	22.00	25.00	16.50	14.16	40.00	31.54	39.07	14.10
Hf	0.70	0.87	0.71	0.43	1.31	1.00	0.89	0.40
Sm	3.10	1.69	1.39	0.89	2.00	1.68	2.06	0.77
Eu	0.82	0.76	0.53	0.33	0.67	0.66	0.69	0.28
Gd	2.10	2.30	1.94	0.77	2.80	1.37	1.40	0.75
Tb	0.32	0.46	0.42	0.20	0.54	0.44	0.39	0.18
Dy	1.80	2.90	2.80	1.51	3.70	3.29	2.63	1.41
Y	10.00	19.30	18.40	8.78	23.00	29.94	11.87	9.25
Ho	0.35	0.72	0.64	0.34	0.81	0.72	0.53	0.30
Er	0.91	2.00	1.90	0.95	2.50	2.00	1.55	1.00
Tm	0.13	0.30	0.28	0.14	0.33	0.29	0.22	0.16
Yb	0.76	1.82	1.83	0.87	2.20	1.75	1.26	1.09
Lu	0.12	0.27	0.27	0.12	0.33	0.26	0.19	0.17

i; SMC = Southern Domain

Ce83-77	Vp83-79	Pey83-82	BR 6	BR 9	BR 12	Ms 15	AL 851	AL 852
SMC	SMC	SMC	SMC	SMC	SMC	SMC	SMC	SMC
0.02	0.03	0.08	0.03	0.09		0.05	0.92	5.18
0.16	0.14	1.53	0.17	4.82		0.27	10.53	61.10
0.03	0.57	0.27	0.38	0.75	0.01	1.02	0.39	0.76
0.15	0.19	0.23	0.09	0.51	0.00	0.25	0.07	0.23
2.14	7.79	3.93	4.73	2.81	0.09	6.89	5.06	22.79
0.01	0.06	0.02	0.07	0.02	0.02	0.04	0.07	0.25
0.16	3.26	3.01	2.20	13.53	0.74	11.28	1.78	11.45
0.99	8.70	2.98	4.36	15.81	3.25	21.08	4.91	31.70
0.18	0.40	0.55	0.71	0.64	0.04	0.58	0.87	4.18
0.27	1.41	0.62	0.81	1.18	0.63	1.84	0.81	4.46
24.2	125.6	53.6	36.2	104.2	67.0	158.0	74.3	179.3
2.14	7.79	3.93	4.73	2.81	3.80	6.89	5.06	22.79
13.14	48.03	26.51	32.58	4.11	29.80	21.79	40.93	88.52
0.61	1.41	0.77	1.17	0.18	0.86	0.62	1.55	2.54
1.05	2.20	1.62	2.06	0.31	1.54	1.37	1.78	4.23
0.49	0.88	0.66	0.83	0.11	0.62	0.51	0.72	1.52
1.57	3.28	2.57	2.63	0.32	2.20	1.32	2.03	3.14
0.34	0.47	0.41	0.52	0.07	0.44	0.30	0.49	0.63
2.36	3.29	3.28	3.98	0.47	2.94	2.09	3.70	3.85
12.52	16.98	17.40	19.94	2.46	19.20	12.48	22.65	21.12
0.52	0.67	0.75	0.84	0.10	0.67	0.45	0.83	0.81
1.44	1.87	2.13	2.56	0.30	1.95	1.31	2.54	2.32
0.23	0.27	0.29	0.34	0.05	0.28	0.18	0.36	0.34
1.48	1.81	2.07	2.42	0.36	1.85	1.09	2.29	1.98
0.24	0.25	0.30	0.30	0.07	0.27	0.17	0.35	0.30

Z4	Z 7	Z 8	Z 10	Z 28	Z 42	RP83-72	RP87-2	RP91-20
SMC	SMC	SMC	SMC	SMC	SMC	SMC	SMC	SMC
1.50	0.09	0.05	0.04		0.04			
56.93	1.16	0.35	0.26		0.26			
3.24	2.21	0.17	0.82	0.72	0.34	2.80	0.02	0.02
3.96	0.58	0.09	0.66	0.33	0.09	0.51	0.02	0.02
8.72	6.99	3.53	0.27	0.13	6.10	0.15	0.05	0.08
0.06	0.01	0.04	0.02	0.01	0.06	0.03	0.02	0.02
34.94	28.37	12.14	5.96	3.80	2.26	20.00	0.34	0.12
39.09	34.37	19.20	3.98	3.70	6.01	58.00	2.35	1.11
6.65	0.72	0.47	1.46	0.67	1.15	0.67	0.18	0.70
3.33	2.68	1.49	0.20	0.07	1.03	6.70	0.62	0.34
174.5	282.5	98.5	24.4	20.7	57.2	353.0	49.0	24.0
8.72	6.99	3.53	0.27	0.42	6.10	22.00	3.61	2.50
15.61	0.22	2.76	0.18	0.07	38.68	22.00	25.00	16.50
1.20	0.03	0.08	0.05	0.01	1.63	0.70	0.87	0.71
1.34	0.53	0.44	0.11	0.18	2.26	3.10	1.69	1.39
0.61	0.21	0.19	0.05	0.06	1.02	0.82	0.76	0.53
6.21	0.63	0.83	0.48	0.41	3.42	2.10	2.30	1.94
0.55	0.06	0.13	0.10	0.10	0.69	0.32	0.46	0.42
3.84	0.48	0.99	1.00	0.97	5.23	1.80	2.90	2.80
11.95	3.65	6.19	6.95	7.00	23.28	10.00	19.30	18.40
0.96	0.12	0.23	0.29	0.23	1.19	0.35	0.72	0.64
3.26	0.39	0.74	0.91	0.78	3.21	0.91	2.00	1.90
0.50	0.06	0.12	0.15	0.12	0.45	0.13	0.30	0.28
3.92	0.46	0.84	1.02	0.92	3.06	0.76	1.82	1.83
0.40	0.07	0.12	0.14	0.12	0.45	0.12	0.27	0.27

BO83-74	Ta 7	Ta 13	Ta 19	Gr83-75	Ce83-77	Vp83-79	Pey83-82	BR 6
SMC	SMC	SMC	SMC	SMC	SMC	SMC	SMC	SMC
0.01		0.03	0.02	0.02	0.02	0.03	0.08	0.03
0.05		0.31	0.27	0.09	0.16	0.14	1.53	0.17
0.02	0.90	0.56	0.74	0.05	0.03	0.57	0.27	0.38
0.01	0.24	0.27	0.21	0.02	0.15	0.19	0.23	0.09
2.17	0.70	8.86	7.49	2.42	2.14	7.79	3.93	4.73
0.04	0.02	0.01	0.09	0.04	0.01	0.06	0.02	0.07
0.65	6.70	1.84	11.42	1.12	0.16	3.26	3.01	2.20
2.08	7.20	5.69	19.67	3.39	0.99	8.70	2.98	4.36
0.12	1.20	0.49	0.31	0.24	0.18	0.40	0.55	0.71
0.36	0.90	0.68	2.78	0.53	0.27	1.41	0.62	0.81
28.7	103.0	55.7	240.4	24.7	24.2	125.6	53.6	36.2
2.17	4.30	8.86	7.49	2.42	2.14	7.79	3.93	4.73
14.16	40.00	31.54	39.07	14.10	13.14	48.03	26.51	32.58
0.43	1.31	1.00	0.89	0.40	0.61	1.41	0.77	1.17
0.89	2.00	1.68	2.06	0.77	1.05	2.20	1.62	2.06
0.33	0.67	0.66	0.69	0.28	0.49	0.88	0.66	0.83
0.77	2.80	1.37	1.40	0.75	1.57	3.28	2.57	2.63
0.20	0.54	0.44	0.39	0.18	0.34	0.47	0.41	0.52
1.51	3.70	3.29	2.63	1.41	2.36	3.29	3.28	3.98
8.78	23.00	29.94	11.87	9.25	12.52	16.98	17.40	19.94
0.34	0.81	0.72	0.53	0.30	0.52	0.67	0.75	0.84
0.95	2.50	2.00	1.55	1.00	1.44	1.87	2.13	2.56
0.14	0.33	0.29	0.22	0.16	0.23	0.27	0.29	0.34
0.87	2.20	1.75	1.26	1.09	1.48	1.81	2.07	2.42
0.12	0.33	0.26	0.19	0.17	0.24	0.25	0.30	0.30

BR 9	Mb 1	Mb 8	Mb 9	Mb 36	Mb 47	Mb 50	Mb 57	Bt 1
SMC	NMC	NMC	NMC	NMC	NMC	NMC	NMC	NMC
0.09		0.62	0.01	0.02				
4.82		25.85	0.29	0.15				
0.75	2.34	5.39	0.07	0.02	0.10	0.03	3.10	0.23
0.51	1.20	1.03	0.55	0.02	0.68	0.27	0.93	0.07
2.81	0.01	5.35	0.04	0.01	0.36	0.01	0.01	0.16
0.02	0.01	0.01	0.02	0.00	0.02	0.01	0.01	0.01
13.53	42.40	27.36	5.24	0.16	3.01	2.90	49.87	3.10
15.81	24.93	31.96	0.70	0.04	0.42	0.59	71.10	9.70
0.64	1.05	0.90	0.59	0.19	0.59	0.36	0.99	1.00
1.18	0.51	2.16	0.01	0.01	0.02	0.01	2.93	1.18
104.2	454.0	768.6	64.0	9.6	53.3	30.1	468.7	355.0
2.81	0.49	5.35	0.04	0.01	0.08	0.04	3.85	4.70
4.11	0.02	0.16	0.12	0.02	0.15	0.01	3.01	12.10
0.18	0.02	0.06	0.04	0.04	0.15	0.02	0.13	0.24
0.31	0.07	0.27	0.10	0.07	0.19	0.07	0.27	1.04
0.11	0.03	0.11	0.09	0.03	0.08	0.03	0.10	0.32
0.32	0.25	0.39	0.41	0.18	0.65	0.34	0.36	0.75
0.07	0.06	0.05	0.09	0.04	0.12	0.07	0.07	0.12
0.47	0.60	0.47	0.94	0.43	1.23	0.87	0.50	0.72
2.46	4.40	3.33	5.92	2.81	6.80	6.40	3.27	4.80
0.10	0.14	0.10	0.22	0.10	0.29	0.22	0.11	0.16
0.30	0.52	0.39	0.76	0.34	0.88	0.75	0.38	0.50
0.05	0.08	0.07	0.11	0.05	0.21	0.11	0.05	0.08
0.36	0.59	0.54	0.90	0.40	1.10	0.85	0.44	0.59
0.07	0.08	0.08	0.13	0.05	0.11	0.12	0.06	0.09

Bt 3 NMC	Bt 11 NMC	Bt 14 NMC	Bt 19 NMC	Bt 27 NMC	Bt 39 NMC	Bt 40 NMC	FR 9 NMC	FR 10 NMC
0.13	0.02	0.03	0.07	0.01			11.13	
0.14	0.20	1.03	0.80	0.02			82.13	
0.13	0.02	0.26	0.28	0.05	0.56	0.28	0.82	0.05
0.12	0.02	0.05	0.03	0.02	0.13	0.08	0.37	0.04
0.64	1.78	6.69	2.23	0.56	1.50	0.05	1.26	0.24
0.01	0.01		0.04	0.00	0.19	0.01	0.07	0.02
1.28	0.73	2.36	3.15	0.44	4.83	3.20	2.79	1.13
1.77	2.40	8.11	6.03	1.11	11.70	8.50	3.62	3.40
0.33	1.21	0.09	0.83	0.96	0.40	0.28	2.43	0.10
0.17	0.39	1.40	0.60	0.14	1.36	1.21	0.34	0.62
31.8	417.7	290.0	340.6	40.8	99.0	46.0	12.4	34.2
0.64	1.78	6.69	2.23	0.56	5.19	5.90	1.26	3.60
1.12	10.26	5.75	3.59	1.36	19.00	41.00	63.70	26.30
0.05	0.39	0.14	0.13	0.06	0.44	1.33	1.14	0.32
0.19	0.42	1.54	0.32	0.23	1.03	1.89	0.26	0.89
0.08	0.20	0.51	0.19	0.09	0.34	0.67	0.13	0.28
0.27	0.46	1.19	0.44	0.41	1.20	2.19	0.26	0.70
0.06	0.07	0.15	0.09	0.09	0.25	0.41	0.05	0.10
0.48	0.50	0.83	0.62	0.74	1.65	2.50	0.45	0.62
2.95	3.22	4.29	3.66	4.12	11.50	15.60	4.19	3.50
0.11	0.11	0.16	0.13	0.18	0.41	0.54	0.13	0.12
0.39	0.38	0.43	0.45	0.51	1.24	1.56	0.49	0.35
0.06	0.07	0.07	0.07	0.08	0.18	0.21	0.08	0.05
0.46	0.46	0.38	0.53	0.55	1.21	1.38	0.56	0.42
0.07	0.07	0.06	0.08	0.08	0.19	0.20	0.10	0.06

FR 11	ST 2	CH 11
NMC	NMC	NMC
	0.02	
	0.23	
0.86	3.25	0.15
0.37	1.05	0.12
0.87	1.11	0.01
0.03	0.01	0.03
6.60	38.17	1.94
14.10	61.86	1.71
0.16	0.35	0.31
1.46	0.27	0.13
56.6	306.4	17.7
5.95	1.11	0.73
26.50	0.09	3.73
0.35	0.04	0.18
1.11	0.15	0.46
0.35	0.08	0.20
0.84	0.34	0.93
0.12	0.13	0.17
0.78	1.16	1.39
4.10	27.95	8.82
0.14	0.30	0.30
0.39	0.92	0.94
0.06	0.14	0.13
0.48	0.89	0.92
0.07	0.15	0.12

Table 2. Trace elements in clinopyroxenes from Lower Silesia (Poland), analysed by LA-ICP-MS.

element	LA74	LA 56	LA 62	LA 81	LA 31	LA 58	LA 39	LA 85
Rb	0.03	0.04	0.10	0.07	0.06	0.25	0.07	0.02
Ba	0.22	0.22	1.62	0.85	0.13	0.13	0.43	0.10
Th	1.51	2.38	0.52	1.82	0.74	0.93	0.56	1.26
U	0.41	0.47	0.15	0.33	0.19	0.26	0.15	0.39
Nb	14.99	2.64	5.87	4.55	2.12	14.21	0.40	3.94
Ta	0.06	0.05	0.02	0.04	0.00	0.10	0.00	0.02
La	21.14	9.55	6.06	14.04	8.42	12.54	4.08	11.89
Ce	48.00	12.34	15.64	18.09	14.54	30.80	4.59	18.15
Pb	0.46	0.62	0.24	0.35	0.48	0.47	0.35	0.34
Pr	4.93	0.96	1.64	1.43	1.05	3.54	0.22	1.43
Sr	220.5	58.4	176.8	179.2	101.3	402.8	25.9	122.7
Nd	14.99	2.64	5.87	4.55	2.12	14.21	0.40	3.94
Zr	2.67	0.48	5.15	15.25	0.18	15.98	0.14	0.59
Hf	0.08	0.08	0.15	0.48	0.04	0.16	0.05	0.02
Sm	1.49	0.38	0.94	0.82	0.12	2.41	0.08	0.31
Eu	0.37	0.15	0.25	0.26	0.04	0.69	0.04	0.10
Gd	0.89	0.79	0.72	0.73	0.24	1.99	0.26	0.38
Tb	0.16	0.17	0.10	0.10	0.05	0.23	0.08	0.08
Dy	1.14	1.54	0.61	0.66	0.56	1.41	0.81	0.65
Y	6.90	8.49	3.47	3.76	4.38	6.69	5.98	4.98
Ho	0.28	0.32	0.12	0.14	0.14	0.24	0.23	0.16
Er	0.90	1.09	0.37	0.39	0.46	0.69	0.78	0.55
Tm	0.14	0.16	0.05	0.06	0.09	0.09	0.12	0.08
Yb	0.92	0.99	0.36	0.38	0.64	0.66	0.82	0.66
Lu	0.17	0.15	0.05	0.05	0.09	0.09	0.13	0.10

LA 83	LA 38	WG 10	Tr 27	LU 50	LU 28	LU 8	LA 67	LA74
0.34	0.05	0.12	0.05	0.04	0.05	0.02	0.33	0.03
0.96	0.28	0.09	0.29	0.26	0.14	0.05	0.10	0.22
0.70	0.26	0.13	0.48	0.24	0.56	0.94	0.85	1.51
0.32	0.14	0.05	0.10	0.07	0.13	0.19	0.26	0.41
2.35	0.57	21.58	24.96	13.93	7.30	11.28	8.89	14.99
0.09	0.01	0.16	0.08	0.04	0.08	0.03	0.10	0.06
8.11	5.95	6.41	10.35	6.43	6.52	11.04	9.43	21.14
12.82	7.23	24.90	32.94	19.45	14.78	27.09	19.40	48.00
0.50	0.28	0.15	0.57	0.20	0.29	0.60	0.79	0.46
1.15	0.33	4.31	5.14	2.99	1.81	3.06	2.17	4.93
57.4	37.8	183.0	368.5	217.1	240.9	445.9	91.9	220.5
2.35	0.57	21.58	24.96	13.93	7.30	11.28	8.89	14.99
1.13	0.58	51.48	138.47	86.29	12.15	7.66	15.52	2.67
0.35	0.02	1.24	2.57	0.97	0.08	0.22	0.20	0.08
0.60	0.13	5.09	6.47	3.12	1.52	1.64	1.35	1.49
0.23	0.02	1.43	2.00	0.99	0.46	0.51	0.39	0.37
1.50	0.14	4.10	5.91	2.47	1.26	1.07	1.21	0.89
0.25	0.05	0.50	0.76	0.35	0.17	0.14	0.18	0.16
1.60	0.28	2.90	5.05	1.99	0.96	0.76	1.14	1.14
11.21	2.25	10.93	22.15	9.04	4.52	3.38	6.32	6.90
0.28	0.08	0.48	0.88	0.35	0.17	0.13	0.20	0.28
1.04	0.24	1.06	2.23	0.90	0.44	0.39	0.60	0.90
0.17	0.06	0.13	0.29	0.11	0.06	0.05	0.09	0.14
0.76	0.34	0.78	1.85	0.65	0.37	0.41	0.66	0.92
0.17	0.09	0.09	0.26	0.08	0.05	0.06	0.08	0.17

LA 56	LA 62	LA 81	LA 31	LA 58	LA 39	LA 85
0.04	0.10	0.07	0.06	0.25	0.07	0.02
0.22	1.62	0.85	0.13	0.13	0.43	0.10
2.38	0.52	1.82	0.74	0.93	0.56	1.26
0.47	0.15	0.33	0.19	0.26	0.15	0.39
2.64	5.87	4.55	2.12	14.21	0.40	3.94
0.05	0.02	0.04	0.00	0.10	0.00	0.02
9.55	6.06	14.04	8.42	12.54	4.08	11.89
12.34	15.64	18.09	14.54	30.80	4.59	18.15
0.62	0.24	0.35	0.48	0.47	0.35	0.34
0.96	1.64	1.43	1.05	3.54	0.22	1.43
58.4	176.8	179.2	101.3	402.8	25.9	122.7
2.64	5.87	4.55	2.12	14.21	0.40	3.94
0.48	5.15	15.25	0.18	15.98	0.14	0.59
0.08	0.15	0.48	0.04	0.16	0.05	0.02
0.38	0.94	0.82	0.12	2.41	0.08	0.31
0.15	0.25	0.26	0.04	0.69	0.04	0.10
0.79	0.72	0.73	0.24	1.99	0.26	0.38
0.17	0.10	0.10	0.05	0.23	0.08	0.08
1.54	0.61	0.66	0.56	1.41	0.81	0.65
8.49	3.47	3.76	4.38	6.69	5.98	4.98
0.32	0.12	0.14	0.14	0.24	0.23	0.16
1.09	0.37	0.39	0.46	0.69	0.78	0.55
0.16	0.05	0.06	0.09	0.09	0.12	0.08
0.99	0.36	0.38	0.64	0.66	0.82	0.66
0.15	0.05	0.05	0.09	0.09	0.13	0.10